Journal of Hydrology 573 (2019) 406–421

Contents lists available at ScienceDirect

Journal of Hydrology

journal homepage: www.elsevier.com/locate/jhydrol

Research papers

Improvement of land surface model simulations over India via data assimilation of satellite-based soil moisture products

Akhilesh S. Nair[a], J. Indu[a,b,*]

[a] Department of Civil Engineering, Indian Institute of Technology Bombay, Mumbai 400076, India
[b] Interdisciplinary Center for Climate Studies, Indian Institute of Technology Bombay, Mumbai 400076, India

ARTICLE INFO

This manuscript was handled by Dr Emmanouil Anagnostou, Editor-in-Chief, with the assistance of Viviana Maggioni, Associate Editor

Keywords:
Land data assimilation
Soil moisture
ASCAT
SMOS-IC
ESA CCI

ABSTRACT

Realistic representation of surface states using the land surface model (LSM) is extremely challenging owing to human-induced changes and uncertainty in forcing data. In this study, we focus on two crucial objectives pertaining to hydrology namely (a) to understand the ability of different soil moisture (SM) products to improve simulation of unmodeled irrigation processes through data assimilation process, and (b) to learn the feasibility of these SM products to correct the spatial surface soil moisture artifacts caused due to error in precipitation forcing. The utility of SM products evaluated in the present study are retrieved from different satellite sensors and algorithms such as the active satellite-based the Advanced Scatterometer (ASCAT), merged SM from European Space Agency Climate Change Initiative (ESA CCI V4.2) and the latest passive microwave-based SMOS INRA-CESBIO (SMOS-IC) SM product. The results presented for three years (2010, 2011 and 2012) suggest that assimilation of ASCAT and CCI based products effectively captures the SM changes due to irrigation. Similarly, it corrects the spatial artifacts caused due to precipitation errors. However, the single sensor based products have a limitation in spatial samples per day which is critical to capture dynamic SM products over a larger area. Hence, blended products are more effective on a larger area to capture the dynamics in a more effective manner at daily temporal resolutions.

1. Introduction

Soil moisture (SM) is a crucial surface state variable that plays a decisive role in the exchange of water and energy fluxes over the land and atmospheric continuum. It has a prominent influence on various climate processes like precipitation (Koster et al., 2004; Crow et al., 2011; Pellarin et al., 2013; Ciabatta et al., 2017; Aghakouchak et al., 2012), air temperature (Miralles et al., 2014), stream flow and groundwater (Nair and Indu, 2018a; Ahmed et al., 2016). This is mainly as SM dictates the partitioning of rainfall to infiltration and runoff (Botter et al., 2007; Orth and Seneviratne, 2013; Salvucci, 2001) and segregates incident energy to latent and sensible heat fluxes (Koster et al., 2004; Liu et al., 2014). The persistent SM memory also has a huge effect on the forecast skill of droughts (Luo and Wood, 2007), floods (Parinussa et al., 2016), heat waves (Miralles et al., 2014) and thunderstorms (McColl et al., 2017). An accurate assessment of prevailing SM condition remains critical in long range and seasonal numerical weather forecasts (Dirmeyer and Halder, 2016; Koster et al., 2004). In particular, the root zone SM, is extremely important for crop yield forecasting, agricultural drought monitoring (Adegoke and Carleton, 2002; Bolten et al., 2010; Han et al., 2014; Wang et al., 2007) water resources management and climate studies (Chen et al., 1996; Liang et al., 1994; Sellers et al., 1997; Sorooshian et al., 2005).

Past four decades have witnessed the evolution of microwave remote sensing as a promising source of global SM estimates (Nair and Indu, 2018b, Karthikeyan et al., 2017a,b). These SM estimates rely on low-frequency microwave observations owing to its high sensitivity to dielectric properties of the soil-water medium and low attenuation from atmosphere/vegetation. Some of the widely used satellite SM products are the Advanced Scatterometer (ASCAT) aboard Meteorological Operational (METOP) satellites (Wagner et al., 2013), multi-frequency polarimetric microwave radiometer WindSat aboard Coriolis satellite (Gaiser et al., 2004), Advanced Microwave Scanning Radiometer-Earth Observing System (AMSR-E; Njoku et al., 2003) aboard Aqua satellite, Advanced Microwave Scanning Radiometer 2 (AMSR2; Imaoka et al., 2010) aboard the Global Change Observation Mission-Water (GCOM-W) satellite, Soil Moisture Ocean Salinity (SMOS) mission (Kerr et al., 2010) and the Soil Moisture Active Passive (SMAP) mission (Entekhabi et al., 2010). The availability of these SM estimates have led to blended multi-satellite SM products such as the Soil Moisture Operational Products System (SMOPS; Liu et al., 2012; Nair and Indu, 2016) and the European Space Agency's Climate Change Initiative (ESA CCI).

* Corresponding author at: Department of Civil Engineering, Indian Institute of Technology Bombay, Mumbai 400076, India.
E-mail address: indusj@civil.iitb.ac.in (J. Indu).

https://doi.org/10.1016/j.jhydrol.2019.03.088
Received 1 January 2019; Received in revised form 20 March 2019; Accepted 26 March 2019
Available online 27 March 2019
0022-1694/ © 2019 Elsevier B.V. All rights reserved.

Table 1
Details of perturbation attributes used for meteorological forcing inputs and for state variables.

	Variable	Perturbation Type	Standard Deviation	Cross Correlation			
				P	SW	LW	
Forcing	Precipitation (P)	Multiplicative	0.5	1.0	−0.8	0.5	
	Downward Shortwave (SW)	Multiplicative	0.3	−0.8	1.0	−0.5	
	Downward Longwave (LW)	Additive	50	0.5	−0.5	1.0	
				SM1	SM2	SM3	SM4
State Variable	SM Layer1	Additive	6.00×10^{-3}	1.0	0.6	0.4	0.2
	SM Layer2	Additive	1.10×10^{-4}	0.6	1.0	0.6	0.4
	SM Layer3	Additive	6.00×10^{-5}	0.4	0.6	1.0	0.6
	SM Layer4	Additive	4.00×10^{-5}	0.2	0.4	0.6	1.0

Table 2
Summary of observation perturbation parameters.

Satellite Soil Moisture Product	Perturbation Type	Standard Deviation
SMOS IC	Additive	0.04
ASCAT	Additive	0.05
ESA CCI V4.2	Additive	0.04

Table 3
Summary of Triple collocation analysis.

Soil Moisture Product	MERRA Land SM	GLDAS CLSM SM	NODA	ASC	SMOS-IC	CCI
TC 1	✓	✓	✓			
TC 2	✓	✓		✓		
TC 3	✓	✓			✓	
TC 4	✓	✓				✓

Table 4
Contingency table for validating GDAS precipitation with IMD rain gauge data.

	Rain detected by IMD (Yes)	No Rain detected by IMD (No)
Rain detected by GDAS (Yes)	Hit (H)	False (F)
No rain detected by GDAS (No)	Miss (M)	Null event (T)

There exist studies which have simulated SM vertical profiles at various depths using Land surface models (LSM) and near-surface atmospheric forcing data. The modeling community and hydrologists greatly rely on LSMs to recreate complex interactions between land and near surface atmosphere (Rodell et al., 2004), which can estimate water and energy fluxes at high spatial resolution (Zaitchik et al., 2010). Though LSMs estimate surface state variables at high spatiotemporal resolution, they are subjected to uncertainties in forcing data, improper parameterization and inadequate physical processes representations. To facilitate regional scale studies, efforts have been conducted to use data assimilation (DA) techniques to improve LSM simulations using remote sensing data (Kumar et al., 2014; Lievens et al., 2015a,b; Nair and Indu, 2016; Tian et al., 2010) as well as on global scale (Liu and Mishra, 2017; Reichle and Koster, 2005; Rodell et al., 2004; Zhao et al., 2016).

Most LSMs are limited in their representation of human engineered unmodeled processes like irrigation (Kumar et al., 2015; Lawston et al., 2017; Brocca et al., 2018). In order to overcome this, studies have utilized data assimilation (DA) technique to constrain LSM with remote sensing based SM observations (De Lannoy and Reichle, 2016; Lievens et al., 2015a,b). The study by Kumar et al. (2015), indicate remote sensing as a promising source to improve irrigation processes, but bias correction technique is a major limiting factor to use remote sensing observations to correct for unmodeled processes. On the other hand, a recent study by Blankenship et al. (2018) indicated that assimilation of SM corrects the spatial artifacts caused due to uncertain precipitation. Which has motivated us to formulate two crucial and linked objectives, which are a) Improving the simulation of unmodeled traditional irrigation processes over India and b) Correcting SM error caused due to the LSM forcing uncertainty related to precipitation spatial artifacts.

In this study, we check the effect of DA on three different SM products namely the active scatterometer based SM from ASCAT, the passive radiometer based SM from SMOS-IC, and multi-satellite blended SM from ESA CCI V4.2. These products are adopted for assimilation experiments in order to learn the ability of different sensor frequencies to furnish our objectives i.e. ASCAT SM is retrieved from C-band sensors while SMOS-IC relies on L-band sensors. Similarly, it will provide further insight into the impact of sensor footprint on SM assimilation as ASCAT has a higher footprint (~25 km) compared to coarser SMOS footprint (~40 km). Further, the third product (ESA CCI) is selected in order to verify the utility of blended SM product. This is important as blended products have the highest temporal and spatial samples compared to single sensor SM products.

2. Model and data description

2.1. Noah LSM

The present study relies on version 3.6 of Noah model (Mitchell, 2004) to simulate land surface states over the Indian subcontinent (similar to Nair and Indu, 2016) at a spatial resolution of 0.25° × 0.25°. It relies on the modified Penman-Monteith equation to estimate the diurnal variation of the atmospheric resistance coefficient (Chen et al., 1996; Mahrt and Ek, 1984). This model has a four-layer configuration for SM and temperature extending to a total depth of 2 m from the surface to bottom. The soil layer depths are set at 10 cm, 30 cm, 60 cm, and 100 cm so as to capture the daily, weekly, and seasonal evolution of SM (Chen and Dudhia, 2001). As such, surface layer estimates from model represents the SM from the first 10 cm, which is deeper than the monitoring depth of satellite-based sensors. Some of the previous studies have evaluated the effect of changing the Noah first layer depth from 10 cm to 5 cm. They have suggested that reducing the first layer depth has minimal impact on the SM estimation and that the difference between observed SM (from remote sensing) and simulated SM (from LSM) can be attributed to the LSM model structure rather than the difference in their depth (Shellito et al., 2018, 2016). However, these studies pertain to surface layer depth sensitive to L-band sensors such as SMOS and SMAP. Hence, before assimilation, we evaluate the variability in simulated SM after changing it to shallower depth (2 cm) from default configuration of 10 cm. It should be noted that this analysis is performed at 2 cm owing to its proximity to the sensitivity of C-band sensor (ASCAT). The result from our analysis indicates a minor change (less than 4% over the majority of regions as compared SM from 10 cm layer) in SM when first layer depth is reduced to 2 cm. A further detailed discussion of this analysis is provided in Appendix A. From our analysis and previous studies it can be

Table 5
Details of indices used in this study.

Sr. No.	Performance Measure	Formula
1.	Probability of Detection (POD)	$\frac{H}{H+M}$
2.	Volumetric False Alarm Ratio (VFAR)	$\frac{\sum_{i=1}^{n}(GDAS_i \mid (GDAS_i > t \ \& \ IMD_i \le t))}{\sum_{i=1}^{n}(GDAS_i \mid (GDAS_i > t \ \& \ IMD_i > t)) + \sum_{i=1}^{n}(GDAS_i \mid (GDAS_i > t \ \& \ IMD_i \le t))}$
3.	Volumetric miss Index (VMI)	$\frac{\sum_{i=1}^{n}(GDAS_i \mid (GDAS_i \le t \ \& \ IMD_i > t))}{\sum_{i=1}^{n}(GDAS_i \mid (GDAS_i > t \ \& \ IMD_i > t)) + \sum_{i=1}^{n}(GDAS_i \mid (GDAS_i \le t \ \& \ IMD_i > t))}$

t = is the threshold above which VFAR and VMI are calculated. Here, we have used a threshold of 2.5 mm as minimum rainfall intensity as recommended by the India Meteorological Department.

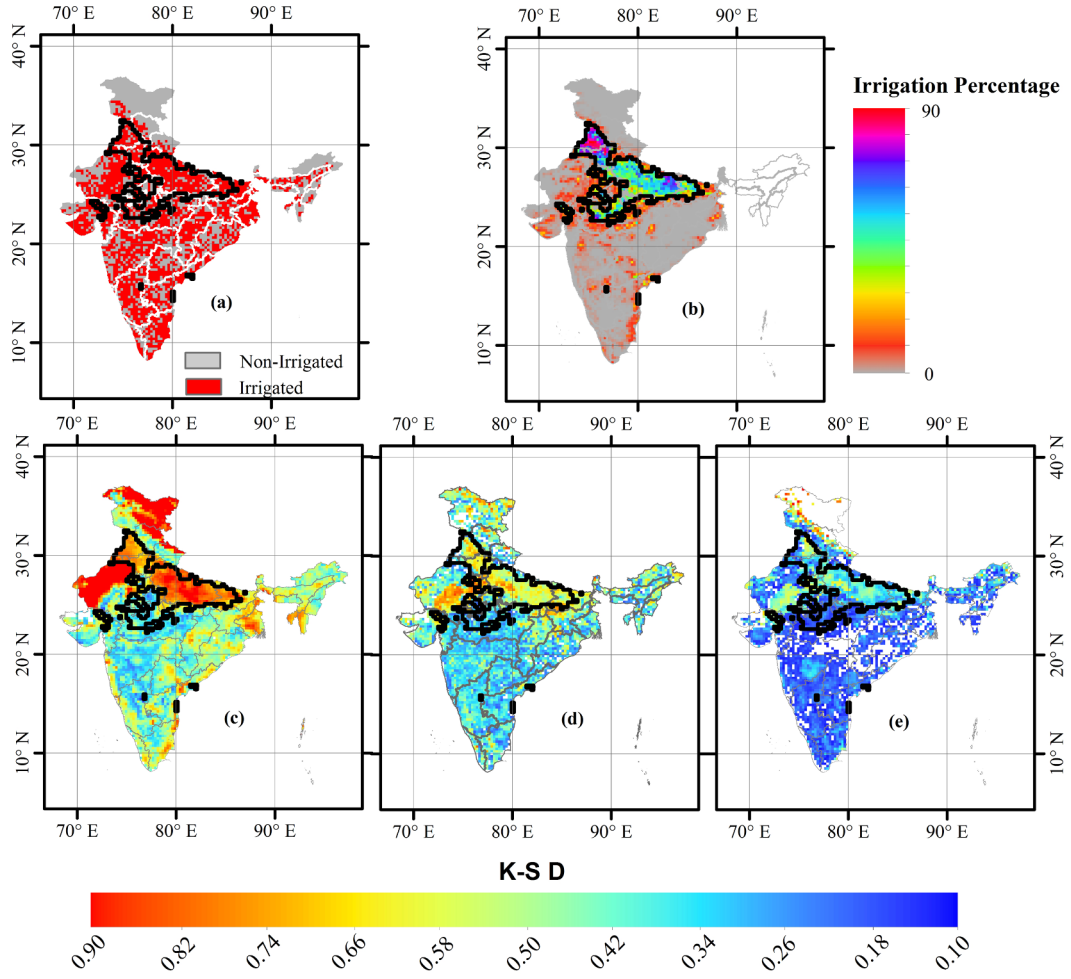

Fig. 1. Depicts (a) Irrigated pixels during a period of three years from 2010 to 2012 (Source: Ambika and Mishra, 2016), (b) Percentage of pixels under winter crop for a duration of three years (Source: Jain et al., 2017), (c) Kolmogorov-Smirnov (K-S) distance between SM without assimilation (NODA) and ASCAT SM (ASC) observations, (d) Kolmogorov-Smirnov (K-S) distance between NODA and SMOS SM (SMOS-IC) observations, (e) Kolmogorov-Smirnov (K-S) distance between NODA and ESA CCI SM (CCI) observations. It is to be noted that the K-S test is performed over datasets from a duration of three years between 2010 and 2012.

inferred that the change in surface layer depth (first layer) of Noah LSM has a nominal impact on soil moisture. Considering all these points and to maintain a uniform Global Land Data Assimilation System (GLDAS) model configuration for intercomparison of assimilation products, the present study adopts the standard model setup (First layer depth of 10 cm). Further, we have adopted a model time step of 15 min for all simulations with output at every one hour. This configuration is most suitable to assimilate different soil moisture products at their instantaneous overpasses. The Noah LSM for the present study is initialized by multi-year spinup by repeated forcing from 1 January 2008 to 31 December 2010 (for seven times), which is equivalent to 21 years simulation. The forcing data for this study stems from GLDAS enhanced NCEP's Global Data Assimilation System (GDAS, Derber et al., 1991).

2.2. Soil moisture dataset description

The present study examines the feasibility of different SM products to improve model efficiency in terms of un-modeled irrigation as well as correction for uncertainty in precipitation forcing. A brief description of the SM products used in the present study is given below. These products are selected with an aim to compare the assimilation skill of passive (SMOS), active (ASCAT) and merged SM (ESA CCI) products to improve LSM simulations.

2.2.1. Passive low-frequency microwave based SMOS-IC SM

The soil moisture estimates from Soil Moisture and Ocean Salinity (SMOS) mission are extracted from multi-angular brightness temperatures

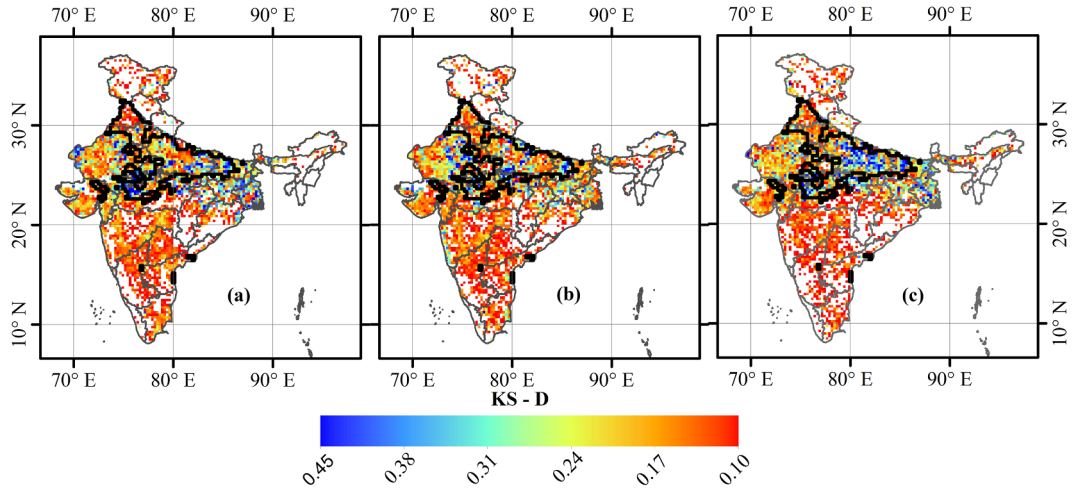

Fig. 2. Kolmogorov-Smirnov (K-S) distance between SM without assimilation (NODA) and ASCAT assimilated SM (ASC), (d) Kolmogorov-Smirnov (K-S) distance between NODA and SMOS assimilated SM (SMOS-IC), (e) Kolmogorov-Smirnov (K-S) distance between NODA and ESA CCI assimilated SM (CCI). It is to be noted that the K-S test is performed over datasets from a duration of three years between 2010 and 2012.

at L-band (1.4 GHz) (Kerr et al., 2010). The conventional operational SMOS level 2 and level 3 algorithms rely on auxiliary files to produce global soil retrieval maps. They further account for correction in antenna pattern and SMOS viewing geometry. Such auxiliary files and processes add to the uncertainty in SM retrievals. However, in this study, we use the latest SMOS product from INRA (Institut National de la Recherche Agronomique) and CESBIO (Center d'Etudes Spatiakes de la BIOsphère). In this product, the sub pixel heterogeneity is neglected in order to avoid uncertainties associated with auxiliary files (Fernandez-Moran et al., 2017a,b; Wigneron et al., 2007). The SMOS-IC product has a similar spatio-temporal resolution as that of operational SMOS level 2 SM product.

2.2.2. Active microwave based ASCAT SM

The ASCAT mission relies on three C-band (5.2 GHz) real aperture radars with vertical polarization configuration to monitor land surface processes. The crucial objective of ASCAT is to monitor global wind direction, however, it has been efficiently used to monitor surface SM owing to its high sensitivity (Figa-Saldaña et al., 2002). The real aperture radar of ASCAT mission has a soil penetration depth of ~1–3 cm depending on soil and atmospheric conditions. It has an improved revisit time of fewer than 2 days and a spatial resolution of 25 Km. For the present study, ASCAT data also stems from SMOPS (Liu et al., 2012).

2.2.3. Blended multi-satellite ESA CCI SM

To evaluate the assimilation skill of blended SM products, the present study utilizes ESA's CCI V4.2 (Dorigo et al., 2017; Gruber et al., 2017; Liu et al., 2012) combined SM products. They are obtained by merging different microwave products captured in the active (e.g., SCAT, ASCAT) and passive systems (e.g., SMMR, SSM/I, TMI, AMSR-E, SMOS, WindSat, AMSR2, SMOS (LPRM), Aquarius, SMAP). The merged products are available at a spatial resolution of 0.25° × 0.25° on the GLDAS v1.0 Noah climatology. The 4.2 version of CCI SM adopts a more advanced and quality controlled data merging technique with additional information as compared to the older versions used by Kumar et al. (2015).

3. DA experimental methodology

The LSM estimates of hydrometeorological variables are known to contain uncertainties due to forcing data and model components. Some of the previous studies have addressed this issue by calibrating the LSM parameters (Franks and Beven, 1999; Franks et al., 1997; Crow, 2003; Corbari et al., 2010; Gutmann and Small, 2010; Corbari and Mancini, 2014; Mishra et al., 2017). However, such methods rely on one variable which has minimal impact on the overall simulation skill of LSM (Gupta et al., 1999). Moreover, the uncertainty in observations used for calibration can result in unrealistic parameters. By assimilating remote sensing observations within LSM, the model prognostic variables (e.g., SM) get updated with respect to observations. The improvement in the prognostic variables through assimilation will be propagated to other hydrometeorological variables through model physics. The present study examines through DA, the performance of different SM products to improve the model simulation skills.

3.1. Assimilation setup and analysis tools

The initialized Noah LSM is simulated for a period of 3 years from 2010 to 2012 (hereafter referred to as study period). As described in Section 2.1, the SM is estimated in 4 soil layers. In order to improve the prediction skill of LSM, first layer SM is involved directly in the DA technique. The daily SM products during the study period are assimilated to improve surface SM of Noah LSM with 1-dimensional Ensemble Kalman filter (EnKF, Reichle et al., 2002; Reichle and Koster, 2004). In the present study, NASA's Land Information System (LIS, Kumar et al., 2006; Peters-Lidard et al., 2007) is used to set up the EnKF assimilation framework. The EnKF algorithm is a sequential assimilation approach which alternates between model forecast stage and state update stage. During the update stage, model states are updated using SM observations based on the Kalman gain factor (Reichle et al., 2002; Kumar et al., 2009, 2012). This depends on the model forecast error variances calculated from the model ensemble. For this, 30 ensembles of the model forecast are generated by imposing random gaussian parameters with zero mean and cross-correlations in perturbation of precipitation and radiation field as shown in Table 1.

Additive Gaussian noise is added to model prognostic variables with vertical correlations for deeper layers. These parameters are based on a study by Nair and Indu, 2016. Since this study adopts the one-dimensional approach of EnKF no spatial correlations are applied. Furthermore, before assimilation, all preliminary analysis indicated that no systematic bias is introduced into the model simulations owing to error parameter configuration in Table 1.

The DA methods rely on the critical assumption of an unbiased model and observation states. However, owing to different approaches of observation (Sensor frequencies) and retrieval algorithms the SM observations are biased with respect to model simulations. Hence, in the present study, all three soil moisture products are preprocessed for bias correction by using CDF matching technique. The observation bias with respect to LSM simulation is removed using a lumped CDF (pixel-wise one CDF for entire year) matching technique (Reichle and Koster, 2004; Reichle et al., 2007; Kumar et al., 2009; Draper et al., 2012; Kumar et al., 2014; Nair and Indu, 2016). As indicated in the study by Kumar et al., 2015, a lumped CDF matching

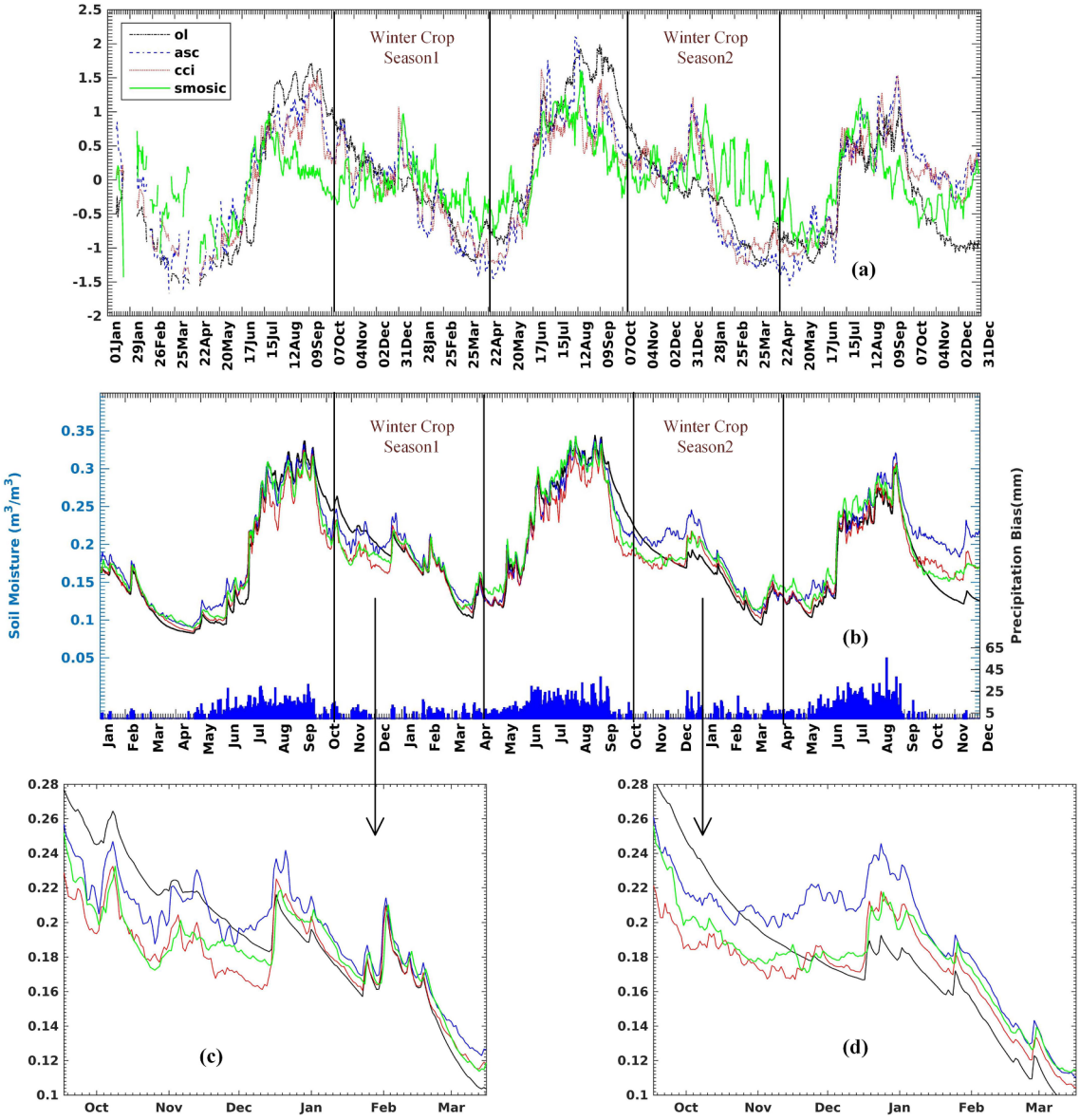

Fig. 3. Represents time series of data over winter irrigated regions (highlighted in Fig. 1b) for (a) Satellite SM observations and NODA, (b) ASC, SMOS-IC, CCI, and NODA SM, (c) same as b but for winter crop season1, (d) same as b but for winter crop season 2.

technique captures the irrigation signals at the cost of a dry bias condition in the non-irrigation period. This bias correction method is adopted over other techniques as over the majority of the Indian states, irrigation is carried out for most of the months. Further, the low sampling frequency and high Radio Frequency Interference (RFI) of SMOS observations add to the problem of computing monthly CDF for all pixels in the study region. Hence, lumped CDF technique is the optimal approach for bias correction in this case.

The SM observations are not assimilated into LSM in the case of (a) snow cover or when the surface temperature is below freezing point (b) when the pixel is covered with dense vegetation, (c) when no convergence is observed in combined SM product (data quality flag). Further, the SM observations are perturbed with random Gaussian noise with parameters as given in Table 2. In order to have effective assimilation, it is verified that the distribution for normalized innovations follows a zero mean and unit standard deviation.

Four different experimental setups are conducted to check the performance of SM assimilation. The details of each are as follows:

(a) NODA: For this setup, Noah LSM is simulated for the study period with a standard setting without any assimilation.

(b) ASC: In this setup ASCAT based SM observations are assimilated into Noah LSM for the study period

(c) SMOS-IC: During this setup, the SMOS-IC SM retrievals are assimilated into Noah LSM for the study period

(d) CCI: In this setup, ESA CCI V4.2 combined (Active + Passive) SM observations are assimilated into Noah LSM for the study period

3.2. Evaluation of SM assimilation results: triple collocation

The first objective of this study is to evaluate the reliability of different SM products to improve simulation of irrigation effects. The results from this assimilation experiments are evaluated using triple collocation (TC) approach (Stoffelen, 1998). In this approach, three mutually independent measurements are used to compute unknown error standard deviations. The main advantage of this approach is that it does not require any measurement as true. The TC approach relies on a linear error model such that the error models are uncorrelated with each other. This approach has been widely used in the field of oceanography (Stoffelen, 1998; Caires and Sterl, 2003; O'Carroll et al., 2008; Gentemann, 2014), hydrology (Roebeling et al., 2012) and particularly in SM studies (Nair and Indu, 2016; Draper et al.,

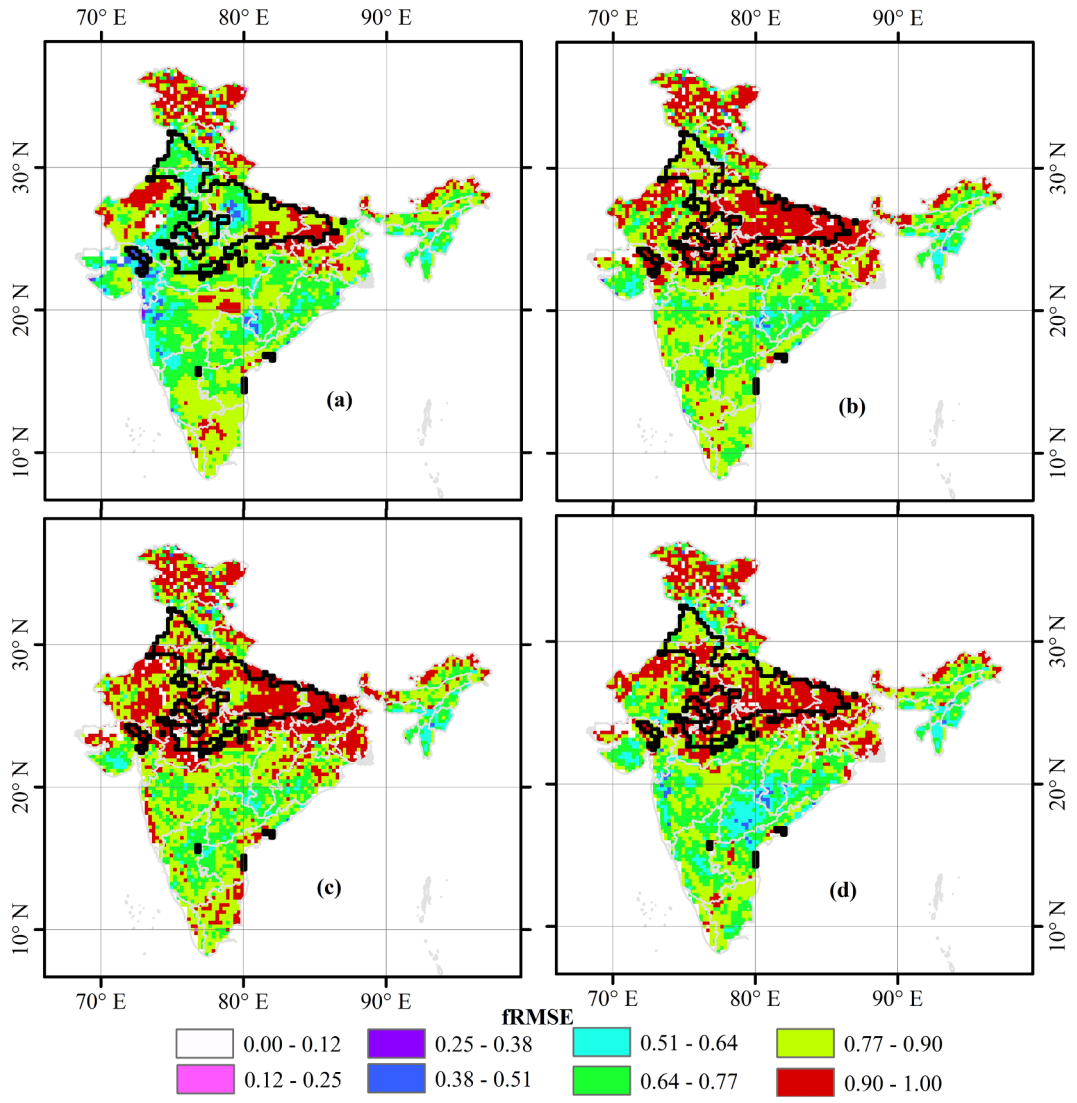

Fig. 4. Depicts fRMSE of SM from triple collocation (TC) technique for a duration of three years (2010–2012) from (a) NODA SM, (b) ASC DA SM, (c) SMOS-IC DA SM, (d) CCI DA SM. Over the winter irrigated regions.

2013; Anderson et al., 2012; Scipal et al., 2008).

The TC furnish a reliable platform for comparison of DA results independent of in-situ soil moisture observations. In order to have independent datasets and avoid correlated errors (crucial assumptions in TC), this study utilizes five SM products for TC analysis as summarized in Table 3. The surface SM products used for analysis stems from MERRA Land, GLDAS CLSM, NODA, ASC, SMOS-IC, and CCI. Here, the last four soil moisture sources are simulated Noah SM and assimilated SMs respectively obtained from the present study. For the analysis, the first two soil moisture products are kept same while the third product is replaced with the NODA and other three assimilated SM results. This approach evaluates assimilation skill within the same reference frame. Detailed analysis of results from TC is provided in Sections 4.1 and 4.2.

The second focus of this study is to evaluate the utility of SM products to improve spatial artifacts caused due to precipitation uncertainty. It is to be noted that the main objective of this analysis is to verify the efficiency of assimilation to improve SM state during missing rainfall events in forcing data rather than the bias in the intensity of rainfall. As a preliminary step towards this, we have validated GDAS precipitation using IMD data.

3.3. Validation of GDAS precipitation

The precipitation data from GDAS are compared with gauge-based precipitation provided by IMD. These are daily rainfall products available at 0.25° × 0.25° resolution over India which is prepared using the 6955 IMD rain gauge stations distributed all over India (Pai et al., 2014). During this analysis performance of GDAS daily precipitation is compared with IMD data using 2 × 2 contingency table as shown in Table 4. This contingency table helps to capture the hits (raining in both datasets), misses (raining in IMD observation but not raining in GDAS precipitation) and False alarms (No rain in IMD but rain in GDAS precipitation). This is used to compute different skill scores including volumetric skill scores (AghaKouchak and Mehran, 2013) such as Probability of Detection (POD), Volumetric False Alarm Ratio (VFAR), and Volumetric Miss Index (VMI) as summarized in Table 5. Here, the bias is computed as the difference of GDAS and IMD precipitation when both the datasets detect rainfall (i.e. during Hit cases).

4. Results

The main focus of this study is to evaluate the effectiveness of SM products to curb uncertainties from the model (Unmodeled irrigation process) and forcing (precipitation). In order to evaluate this, results are presented for different statistical indices utilizing auxiliary datasets. Different regions of India receive rainfall mainly during two monsoon seasons, which are the summer monsoon where it rains in majority of

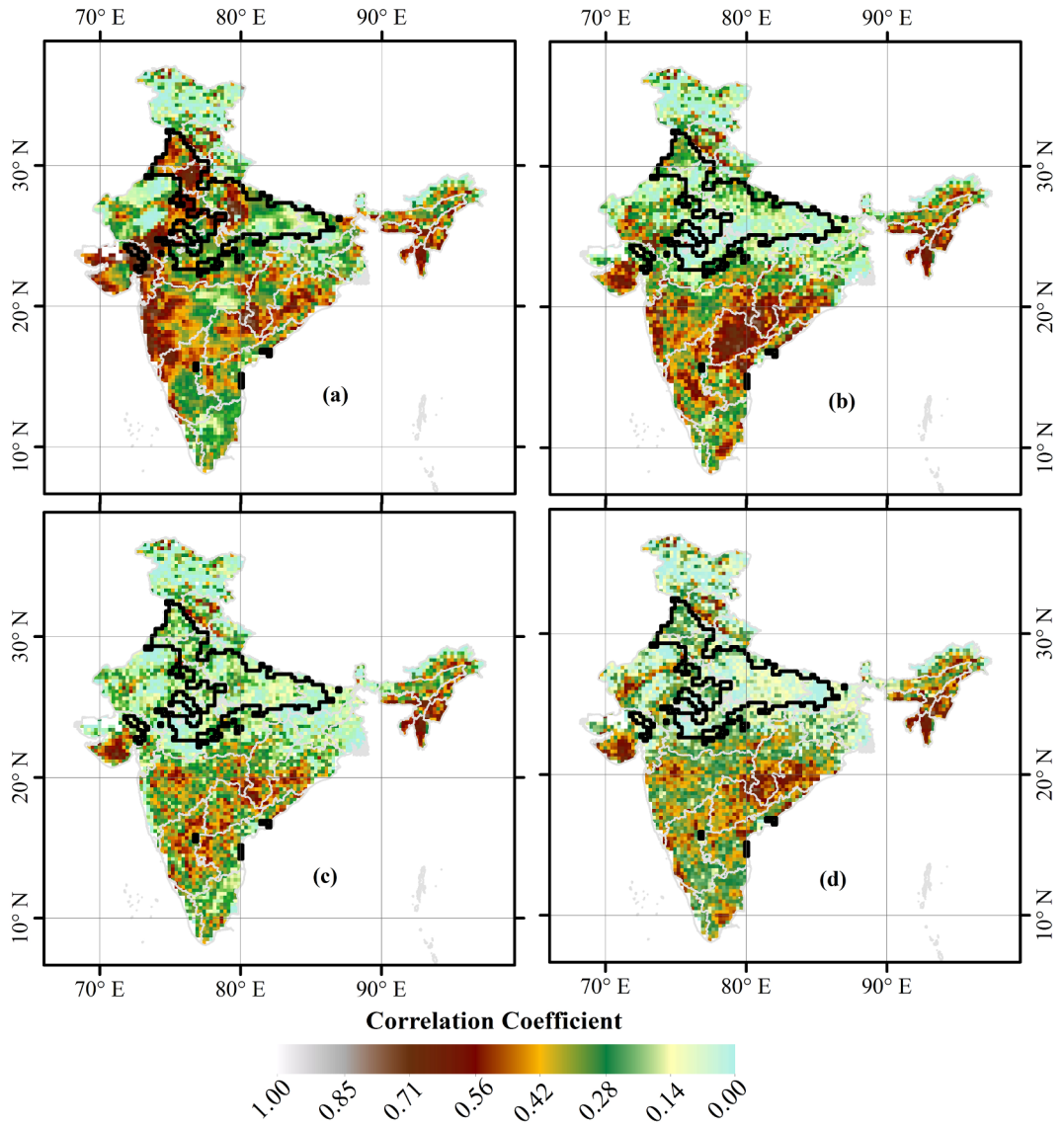

Fig. 5. Depicts Correlation Coefficient (R^2) from triple collocation (TC) technique for a duration of three years (2010 to 2012) from (a) NODA SM, (b) ASC DA SM, (c) SMOS-IC DA SM, (d) CCI DA SM. Over the winter irrigated regions.

Indian states for four months (June, July, August, September) and the second is during retreating monsoon (October, November, December) where the southern peninsula receives most rainfall (Krishnamurthy and Shukla, 2000; Nair and Indu, 2017). Hence, detecting a single irrigation season for whole India is a challenging task as it rains in southern states when irrigation is performed in northern parts. To overcome this issue we selected the winter cropping season (October–March). Fig. 1(b) represents the percentage of pixel area under irrigation between the study period (2010–2012) at a spatial resolution of 1Km. These datasets represent the MODIS based Enhanced Vegetation Index (EVI) for the winter crop season (Jain et al., 2017). Similarly, Fig. 1(a) represents irrigated pixels during the study period (2010–2012) from Ambika and Mishra, 2016, which is obtained using MODIS NDVI at a spatial resolution of 250 m. In order to detect irrigated pixels during the winter season, both datasets are merged into 0.25° × 0.25° and pixels with EVI and irrigation area more than 60% is assumed as irrigated.

4.1. Evaluation of soil moisture over the irrigated region

The assimilation skill of different SM products are evaluated using Kolmogorov-Smirnov (K-S) distance (D). Fig. 1(c–e) represents Kolmogorov-Smirnov (K-S) distance (D) between NODA and satellite soil moisture estimates. The K-S test (Chakravarti et al., 1967) quantitatively compares the probability distribution of two data sets (for example the simulated SM from NODA and ASC). The K-S D computes the distance between empirical distributions of two sample data sets. The K-S test relies on a null hypothesis that both samples originate from the same source distribution. In order to evaluate the ability of the satellite SM products to capture irrigation signals, the K-S test is performed over SM samples during winter irrigation season. The results indicate that all three SM products capture the winter irrigation signals with high K-S D values over major irrigation regions as highlighted in Fig. 1 with a black solid boundary.

To further evaluate the influence of assimilation on SM simulation during winter cropping season K-S test is performed between NODA and assimilated result. The SM estimated are evaluated at a spatial resolution of quarter degree (Model resolution) for a duration of three years. Fig. 2(a) represents K-S D for NODA and ASC assimilated SM, similarly, Fig. 2(b) depicts K-S D between NODA and SMOS-IC, while Fig. 2(c) shows K-S D between NODA and CCI. It should be noted that these results are depicted for only those locations where the null hypothesis for the K-S test is rejected. The smaller D (close to zero) values indicate no difference between the distribution of NODA and assimilated SM products. As this analysis is performed during the winter cropping season, irrigation is the major factor responsible for the difference in SM after

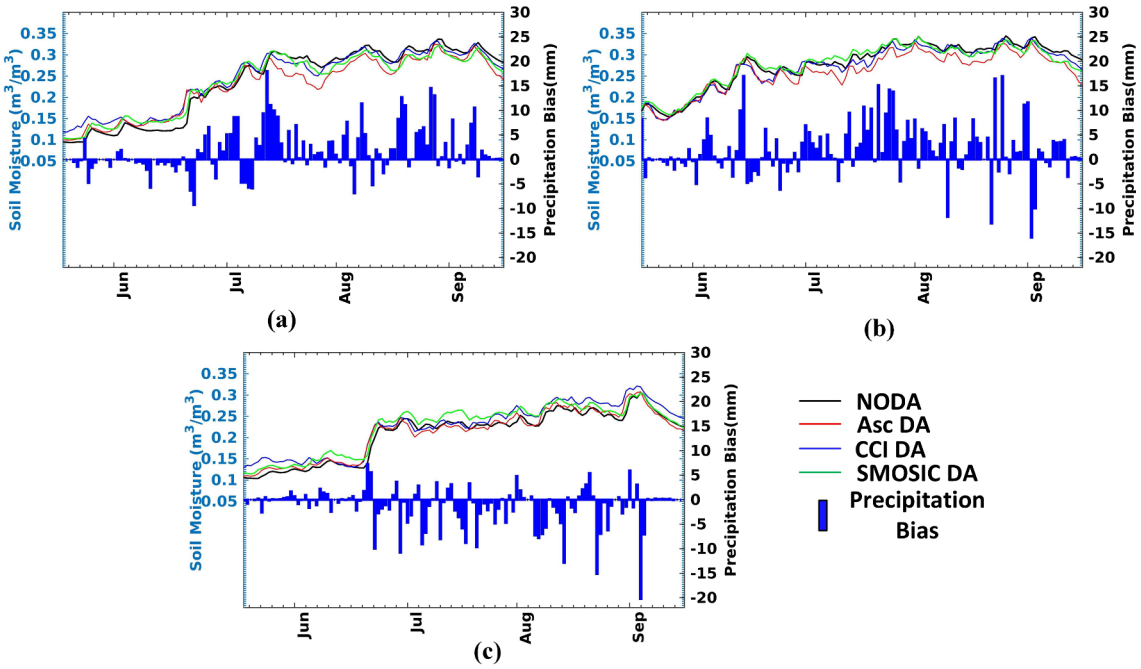

Fig. 6. Shows the time series of SM products during monsoon season (June, July, August, September) for (a) 2010, (b) 2011 and (c) 2012.

assimilation. Which is owing to the absence of precipitation factor as except for the southern peninsula, no other region receives rainfall during this season. Hence, the positive D values (Fig. 2) indicate possible spatial artifacts caused due to the application of irrigation which matches the spatial pattern of irrigated pixels as shown in Fig. 1(a). The point to be noted here is that application of irrigation is not the only reason for large D values, it can occur owing to various factors such as due to change in sensitivity of satellite SM products, uncertainty in retrieval algorithm and forcing data, and model discrepancies (uncertainty in auxiliary files). However, as we are comparing the SM estimates from the same model, hence the contribution from the model and forcing uncertainties can be neglected. In order to eliminate the impact due to the retreating monsoon in southern India, only the northern part of India (as highlighted with solid black boundary line in Fig. 1 b, hereafter referred as irrigated regions) is considered for further irrigation analysis.

Further, in order to confirm that the application of irrigation is responsible for higher K-S D over the irrigated region, we compare the time series plots for SM from remote sensing products and NODA. The first step in this analysis is to normalize all SM products using standard score approach for an equivalent comparison scale. The normalized SM products are then averaged for irrigated pixels for three years as shown in Fig. 3(a). The noise in satellite soil moisture products (Ascat, and SMOS-IC) is reduced by applying a five-day moving average. The NODA indicates a rapid drop in SM after monsoon season for all three years as shown in Fig. 3(a). However, the SM observations indicate a steady SM during the irrigation period particularly during November, December for all three years. Fig. 3(a) indicates that all three SM products are wetter during irrigation season (Winter crop), while it has a dry bias as compared to NODA during monsoon season. The dry bias in SM observations during monsoon season (JJAS) will be discussed in the subsequent session. From these results, it appears that SMOS-IC continuously shows a wet bias during the irrigation period as compared to ASCAT and ESA CCI SM.

To further evaluate the effect of SM assimilation on the Noah LSM simulation trend, a time series is plotted between the assimilated SM products and the NODA results (Fig. 3b). During the winter cropping season 1 (i.e. October 2010–March 2011) NODA has higher SM from October till the first half of Dec (Fig. 3b) as compared to the assimilated product. However, assimilated products indicate a dry SM condition for this period. After december, the assimilated SM increases as compared to NODA, this can be mainly attributed to the impact of irrigation. While the initial wet condition in NODA can be attributed to the high SM during the monsoon season which is analyzed in the subsequent section. During winter cropping season 2 (i.e. October 2011–March 2012) it is observed that NODA SM estimates indicate a rapid decline in the SM after monsoon season while the assimilation products have a constant SM condition during irrigation period and declines after Jan 2012. Therefore, Fig. 3 supports our claim that the assimilation improves the SM condition during the irrigation period as compared. The improvement is particularly prominent over the dry year (October–December 2012), indicating the efficiency of assimilation to increase SM during the irrigation period Fig. 3(b).

The SM estimates from assimilation experiment is further analyzed using triple collocation (TC) technique as explained in Section 3.2. For this analysis, four different TC analysis are initialized using six different SM products as summarized in Table 3. The TC analysis is performed on data during two winter crop seasons from 2010 to 2012. As the modeled SM estimates in the triplets (GLDAS and MERRA) do not include irrigation component, the assimilated SM products will indicate a higher error and low correlation over irrigated regions in TC analysis (Kolassa et al., 2017) This is evaluated by estimating fractional RMSE (fRMSE) as proposed by Draper et al. (2013). Fig. 4 depicts the fRMSE values of SM products derived from TC analysis. The NODA SM product shows lowest fRMSE (Fig. 4a) in the irrigated regions during the winter cropping season, while it increases after SM assimilation (Fig. 4b–d). The increase in fRMSE is particularly prominent over the highly irrigated regions (highlighted with black boundary). The ASC assimilation (Fig. 4c) performs better in term of the widest fRMSE spread throughout the irrigated region as compared to SMOS (Fig. 4b) and CCI (Fig. 4d). This can be attributed to the lowest footprint size of ASCAT sensor as compared to all other products considered in this study. These results are further compared with the squared correlation coefficient (R^2) (McColl et al., 2017; Kolassa et al., 2017). The results of R^2 (Fig. 5) captures the impact of irrigation after assimilation. The NODA case (Fig. 5a) indicates high correlation with GLDAS and CLSM SM over the irrigated region. This is owing to the lack of irrigation component in all these products. The assimilated results from ASC (Fig. 5b), SMOS (Fig. 5c), CCI (Fig. 5d) indicate the lowest correlation over the irrigated regions. This shows the efficiency of the TC method to capture the impact of irrigation after assimilation with high error and low correlation.

As the SM during the initial period of winter cropping season is highly influenced by the preceding monsoon season, an overestimation

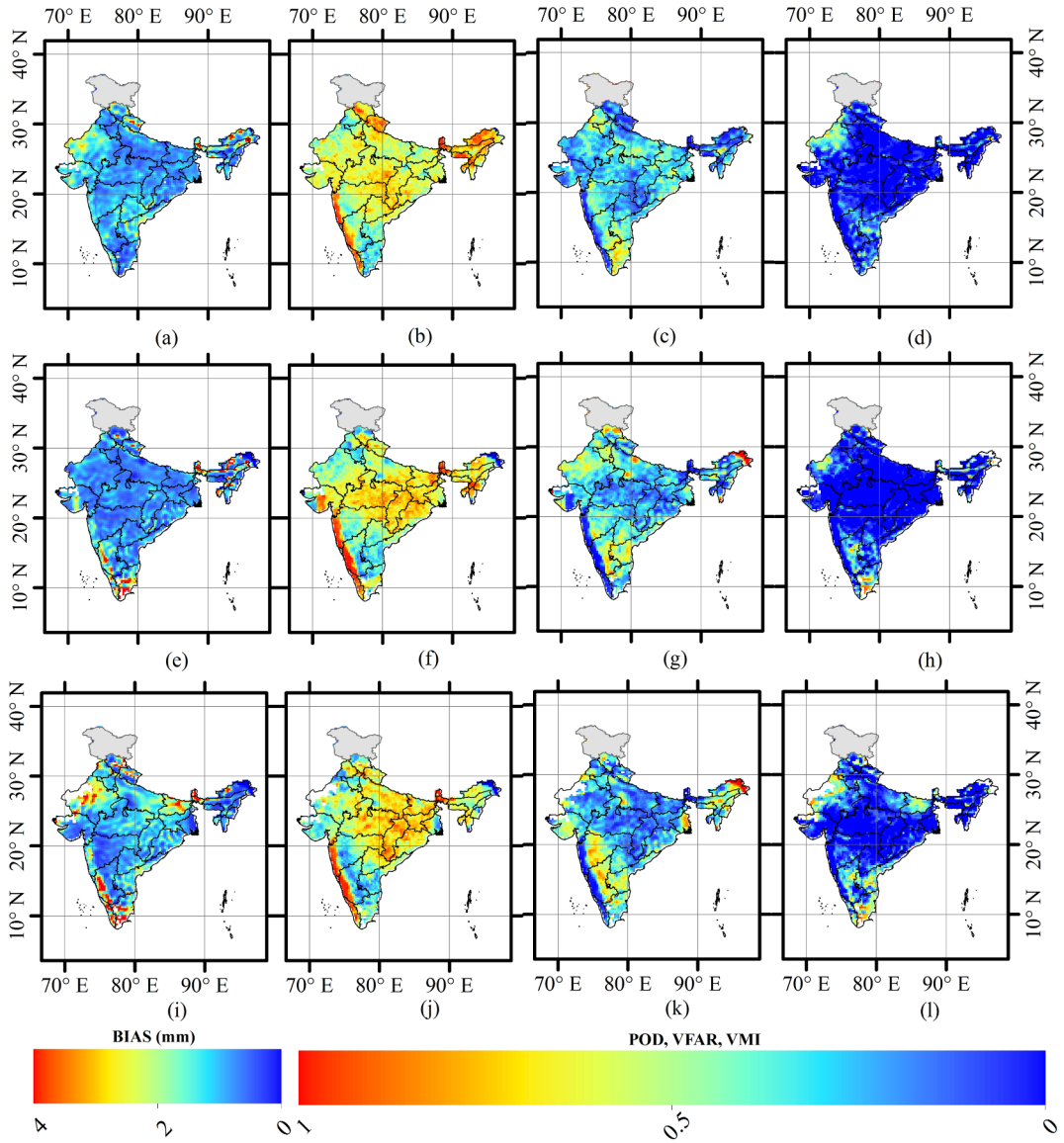

Fig. 7. Precipitation Indices for GDAS precipitation with India Meteorological Department (IMD) precipitation as reference (a) BIAS 2010, (b) POD 2010, (c) VFAR 2010, (d) VMI 2010, (e) BIAS 2011, (f) POD 2011 (g) VFAR 2011, (h) VMI 2011, (i) BIAS 2012, (j) POD 2012, (k) VFAR 2012, (l) VMI 2012. It should be noted that the results over Jammu and Kashmir are masked due to avoid topographic and Snowfall effect.

of precipitation forcing can indicate wet SM condition during the beginning of the winter cropping season as observed in Fig. 2(b). Hence, the second objective of our study is crucial and highly linked to the first objective. In order to evaluate this, we compare the variation in GDAS precipitation forcing and IMD precipitation observation along with SM products from assimilation and NODA.

4.2. Improvement in spatial artifacts due to precipitation uncertainty

Fig. 6 indicates the time series of SM products (NODA, ASC, SMOS-IC, and CCI) and bias in GDAS precipitation over the irrigated region. During the beginning of 2010 monsoon, GDAS has underestimated precipitation as compared to IMD, hence during this period assimilation increases the SM as compared to NODA (Fig. 6a). While for the remaining monsoon season of 2010, GDAS has a positive bias in precipitation, hence the assimilation reduces the SM as compared to NODA. Similar, results can be observed for 2011 (Fig. 6b). During 2012 monsoon (Fig. 6c) the GDAS precipitation has a negative bias for the majority of the days. Due to this assimilation of SM increases the moisture to compensate for the reduced moisture condition due to precipitation forcing. Further, for a detailed analysis of GDAS precipitation, it is validated with IMD data as described in Section 3.3.

Fig. 7 represents the values of indices over the study period. It is observed that the GDAS precipitation has higher VFAR over India throughout the study period. Additionally, it indicates high values of volumetric misses over the southern states and Rajasthan. The significant point to be noted here is that the GDAS precipitation has an overall positive bias as indicated in Fig. 7a, c, i. Owing to this the assimilation of SM observations reduce the SM as compared to wetter NODA estimates (Fig. 3b). Further, from Fig. 7(c, g, k) it can be observed that GDAS precipitation has high VFAR in the central and southeastern coast of India. In order to further quantify the improvement in SM assimilation with uncertainty in precipitation, The TC approach is used to compute RMSE during monsoon season.

Fig. 8 shows the spatial distribution of the mean MISS index and VMI for three years, which signifies the missing rainfall events by GDAS precipitation. Fig. 9 shows the RMSE in SM obtained from TC during the monsoon season of three years. It can be observed that NODA (Fig. 9a) has high RMSE, this pattern matches with the mean MISS index as shown in Fig. 8(a). After ASC assimilation (Fig. 9b) the RMSE is reduced

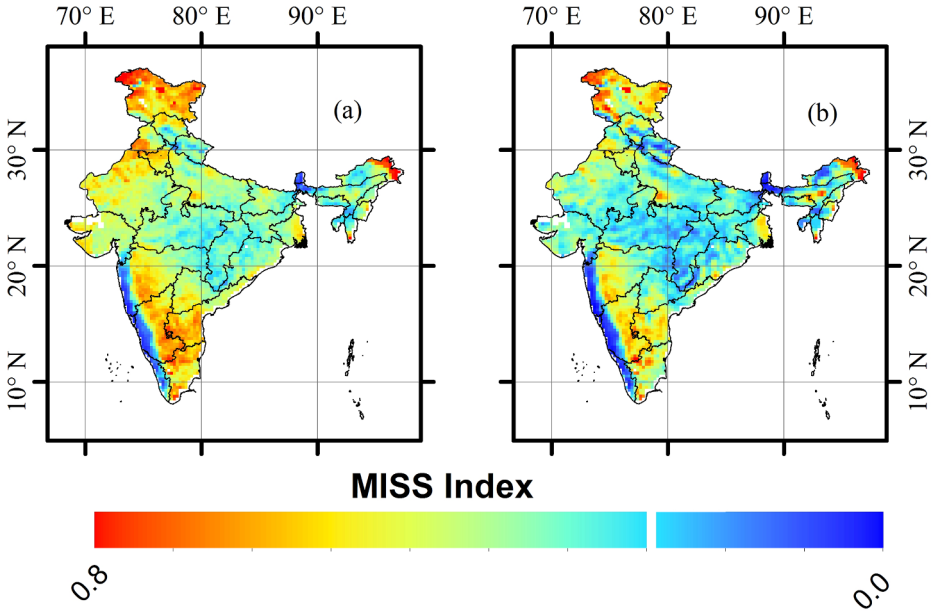

Fig. 8. Shows spatial pattern of mean (a) MISS Index and (b) Volumetric miss index (VMI) for a duration of three years from 2010 to 2012.

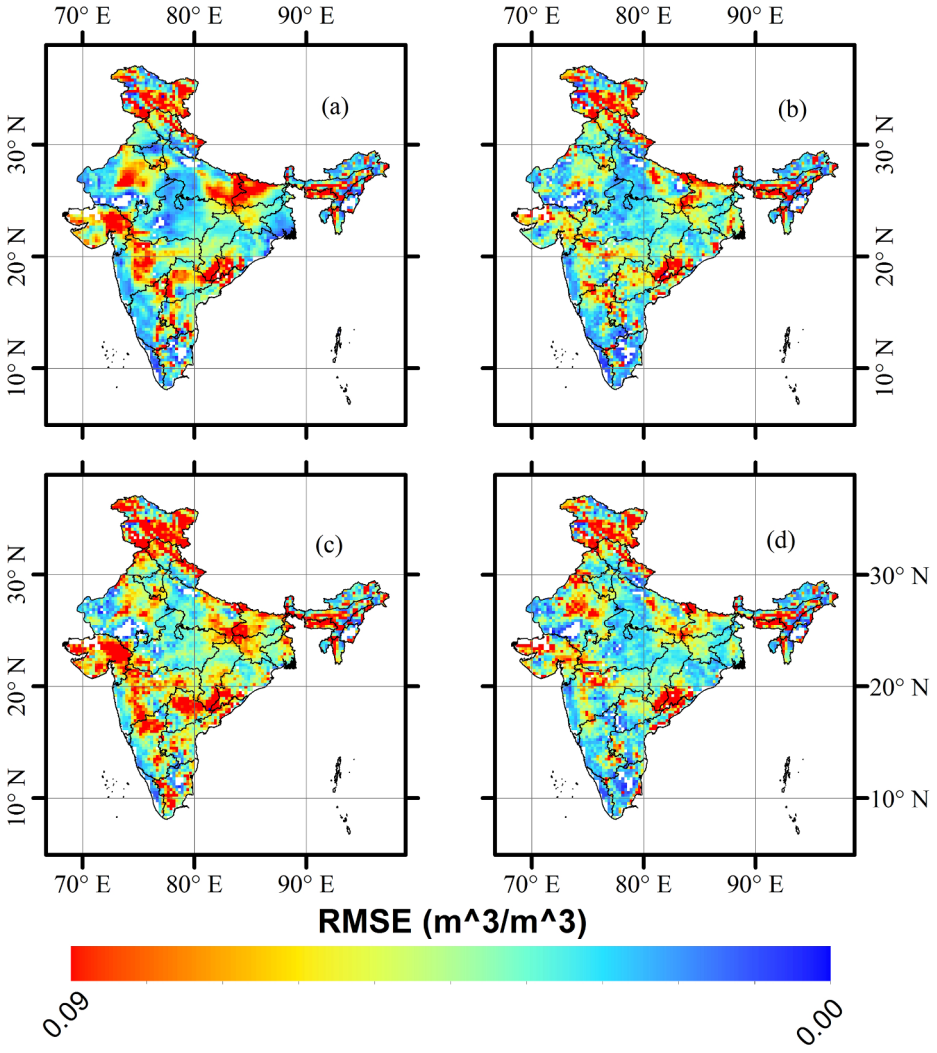

Fig. 9. RMSE of SM obtained from TC for (a) NODA, (b) ASC DA SM, (c) CCI assimilated SM, (d) SMOS-IC DA SM. Which is computed during a period of three years from 2010 to 2012.

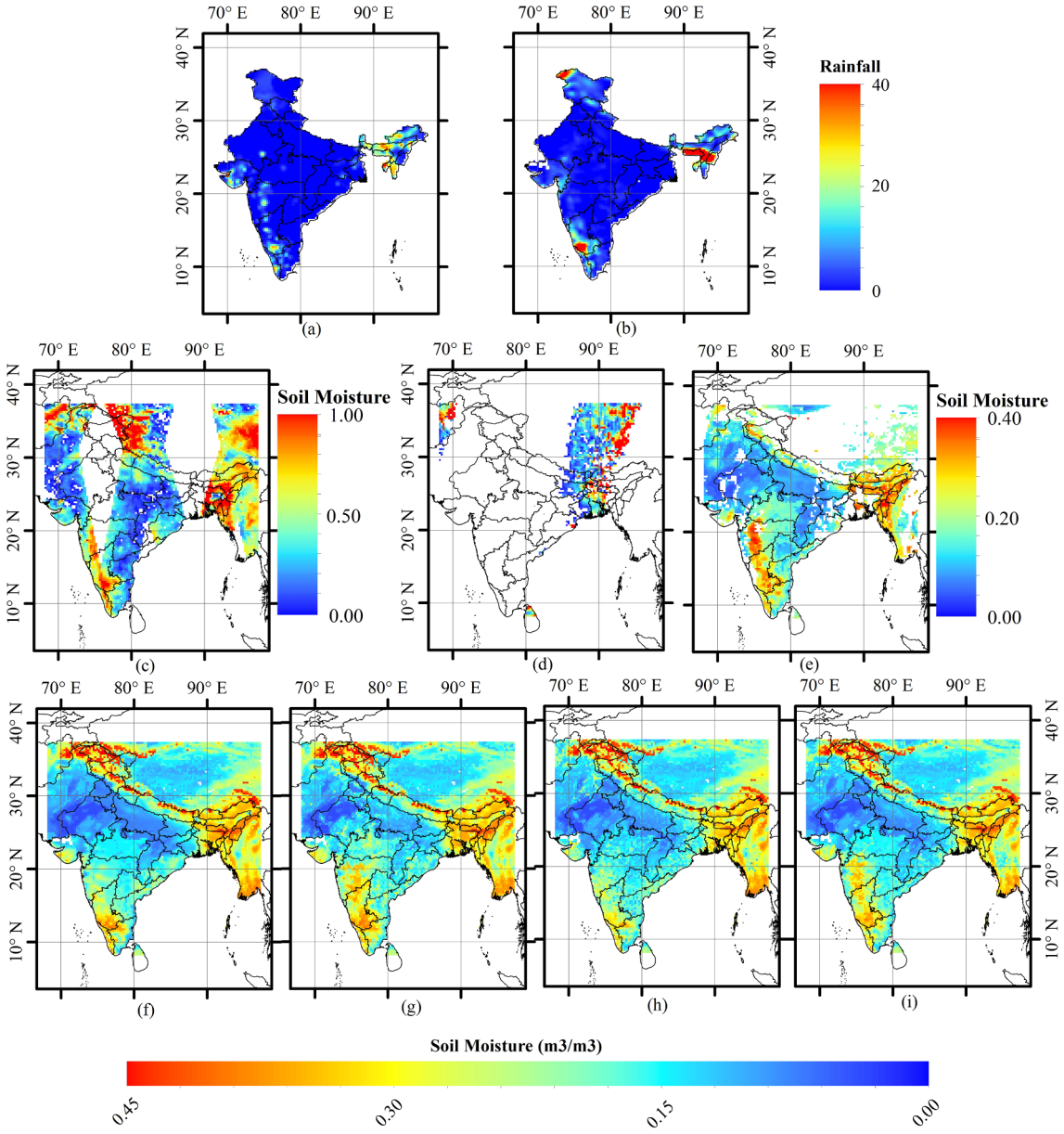

Fig. 10. Depicts (a) Precipitation from India Meteorological Department (IMD), (b) GDAS precipitation, (c) Ascat SM, (d) SMOS-IC SM, (e) ESA CCI SM, (f) NODA SM, (g) SM after ASCAT assimilation, (h) SM after SMOS-IC assimilation (i) SM after ESA CCI assimilation, for 4th June 2010.

considerably. Similarly, assimilation of SMOS-IC (Fig. 9d) reduces the RMSE over pixels with high MISS index. However, assimilation of CCI indicates minimal improvement, as it indicates high RMSE (Fig. 9(c)). This can be attributed to the retrieval approach used for CCI SM, where its CDF is matched with the Noah GLDAS SM.

The present study evaluates the performance of SM assimilation to improve the uncertainty in SM owing to the incorrect precipitation artifacts. For this evaluation, the surface layer soil moisture is compared after one day of missing a rainfall event by GDAS. Since the surface layer has a direct and quick response to rainfall, the assimilation should increase SM than NODA estimates. Although it has a complex hydrological process involving evapotranspiration and surface temperature, we assume that the immediate impact of missing precipitation will be maximum on surface layer soil moisture. Fig. 10 depicts the SM condition for the 3rd of June 2010. It is observed that GDAS (Fig. 10.b) fails to capture rainfall over the state of Maharashtra which is captured by the IMD rain gauges (Fig. 10.a). This rainfall has resulted in high surface SM over regions of Maharashtra as captured in ASCAT (Fig. 10.c) and CCI (Fig. 10.e). However, the SMOS-IC swath fails to capture the high moisture (Fig. 10.d). Therefore, assimilation ASCAT (Fig. 10.g) and CCI (Fig. 10.i) has increased SM over missed rainfall region as compared to NODA case (Fig. 10.f).

Similarly, during 15th June 2011, it is observed that GDAS (Fig. 11.b) shows rainfall over the same region in Maharashtra which is not present in IMD rain gauges (Fig. 11.a). However, ASCAT (Fig. 11.c) has no observation over the region while CCI (Fig. 11.e) indicates a drier patch over the region. The NODA case (Fig. 11.f) shows wet condition over the entire Maharashtra, which is reduced after CCI assimilation (Fig. 11.i).

5. Summary

The present study aims to evaluate the performance of three different soil moisture (SM) products to improve the land surface model (LSM) simulation skill. The SM products used are namely Active satellite-based ASCAT, Passive satellite-based SMOS-IC, and blended multi-satellite product from ESA CCI v4.2 which are assimilated into the Noah LSM. The performance of assimilated products is assessed

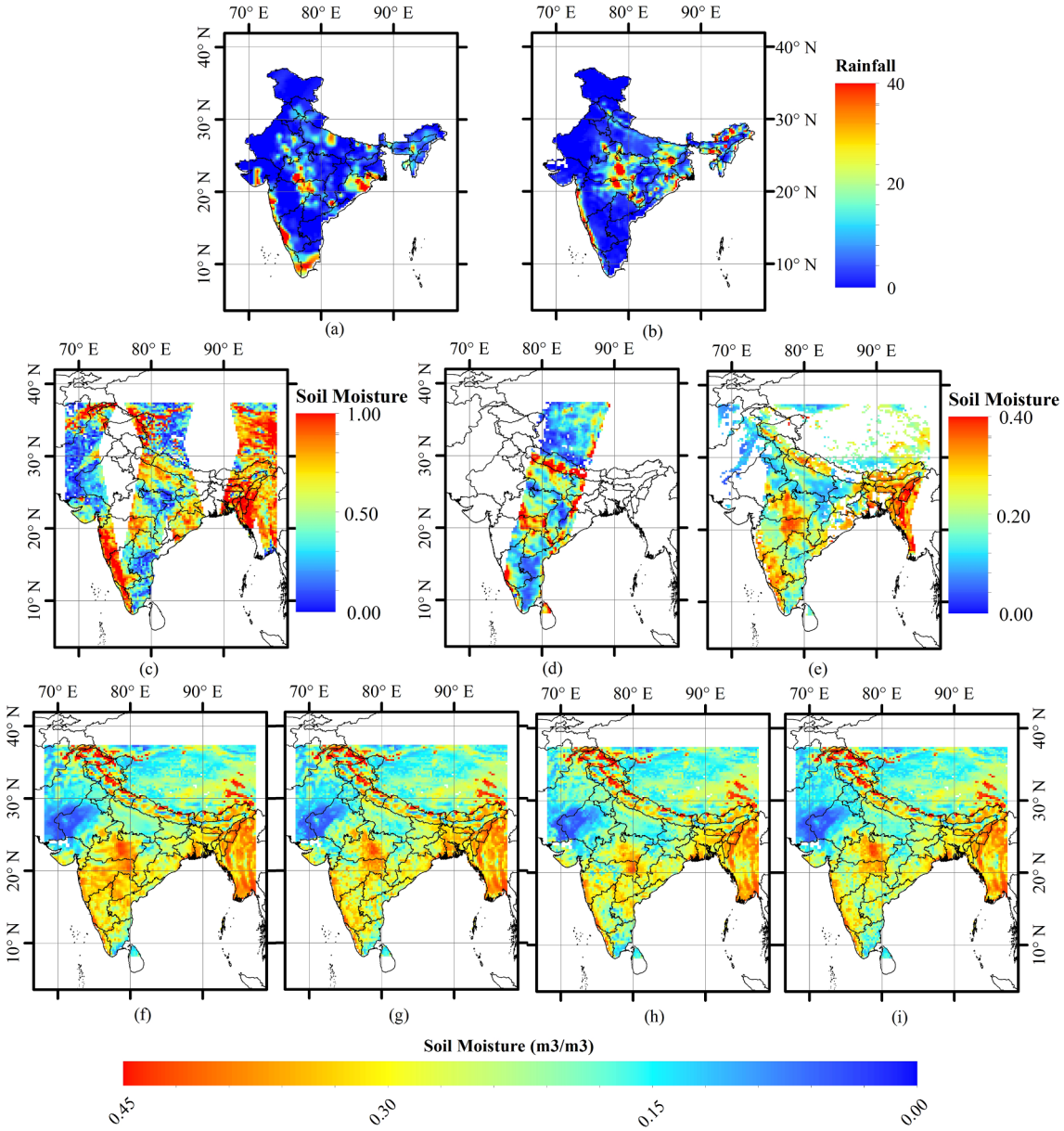

Fig. 11. Depicts (a) Precipitation from India Meteorological Department (IMD), (b) GDAS precipitation, (c) Ascat SM, (d) SMOS-IC SM, (e) ESA CCI SM, (f) NODA SM, (g) SM after ASCAT assimilation, (h) SM after SMOS-IC assimilation (i) SM after ESA CCI assimilation, for 15th June 2011.

focusing on two crucial and linked objectives. The first objective evaluates the performance of SM products to improve the irrigation effect in LSM. And the second objective evaluates the improvement in SM assimilation during ambiguous precipitation forcing.

Seasonal irrigation changes the SM distribution of the region. The impact of irrigation is most prominent in the study region as it consists of the northwestern aquifer, which indicates tremendous decline in groundwater due to irrigation. The satellite SM products detect this irrigation features which can be assimilated into LSM that does not consider irrigation effect. It should be noted that irrigation is not the only cause of high Kolmogorov-Smirnov (K-S) statistic D. However, the seasonal analysis of results indicate irrigation as the primary reason for the variation in SM. This study verifies the effectiveness of SM products to capture irrigation features in assimilated products. The results indicate a similar performance from all three soil moisture products (ASCAT, SMOS-IC, and CCI), though ASCAT and SMOS-IC perform slightly better than CCI in some analysis (especially in RMSE of SM during monsoon). Each of these products have its own advantages such as ASCAT has the smallest footprint size (hence efficient in capturing smaller irrigated fields), SMOS captures data with L-band sensor (highest sensitivity to the surface SM), and ESA CCI has the highest temporal resolution (suitable to capture highly dynamic events).

The second objective of this study evaluates the performance of SM products to improve spatial artifacts due to precipitation uncertainty. For this, the assimilated products are compared to standard LSM simulations. From these results, it can be concluded that ASCAT and SMOS IC assimilation skillfully corrects the uncertainty in SM caused due to an error in precipitation forcing. In addition to these, it can be concluded that the larger temporal samples in CCI are more effective to capture uncertainty in precipitation over a larger area compared to other SM products. This analysis is a qualitative analysis indicating areas showing prominent impact, the future works are planned to quantitatively compare with in-situ SM once data are available.

It is concluded from this study that ASCAT based active SM and SMOS IC SM products have the high ability to improve LSM simulations. But they are affected by longer repeat cycles, resulting in low spatial samples in temporal scales. Similarly, blended CCI SM also effectively captures irrigation and precipitation forcing uncertainty.

However, the CDF matching of combined CCI during final stages of SM generation affects the SM climatology. Hence, it is proposed that new blended products should be generated without projecting it to any particular LSM climatology.

Acknowledgments

Authors thank Sujay V. Kumar and James Geiger of NASA/GSFC for initial setup of the LIS framework over India. Authors acknowledge Hiroko Kato Beaudoing of GLDAS team for processing GDAS data. The authors would like to thank Pierre-Emmanuel Kirstetter for an insightful discussion of results. Authors would also like to thank the editor and anonymous reviewers for constructive suggestions to improve the quality of the manuscript. This work was supported by the Department of Science and Technology, India under the Early career project ECR/2016/001559.

Appendix A. Variability of Noah soil moisture estimates with first layer depth

The primary objective of this study is to evaluate the utility of different SM products to improve the model and forcing uncertainties through assimilation. These products stem from different sensor frequencies such as ASCAT (C-band), SMOS IC (L-band) and ESA CCI (merged multi-satellite product). As different frequencies are sensitive to different depths it is crucial to find the first layer depth of NOAH Land surface model (LSM) before assimilation. As the previous study by Shellito et al. (2018, 2016) indicated low sensitivity of layer depth in SM simulation. But previous studies were conducted by changing depth to 5 cm, which is sensitive depth of the SMOS sensor. However, ASCAT is sensitive to shallower depth (2 cm). Therefore, here we evaluate the impact of layer depth on SM simulation by changing the first layer depth to 2 cm (sensitive depth of ASCAT). Fig. A1(a) indicates a time series of SM for 2 cm and 10 cm first layer depth for a duration of three years from 2010 to 2011. This figure shows that both the layer depths follow the same pattern. The only difference is observed during a dry down period, where 2 cm layer has low SM compared to 10 cm layer. However, the bias is around 0.03 m^3/m^3 which is lesser than the accuracy of satellite SM products (SMOS accuracy 0.04 m^3/m^3). Fig. A1(b) indicates a spatial pattern of percentage bias in SM when changed to 2 cm from 10 cm. It can be observed that the majority of the region have bias

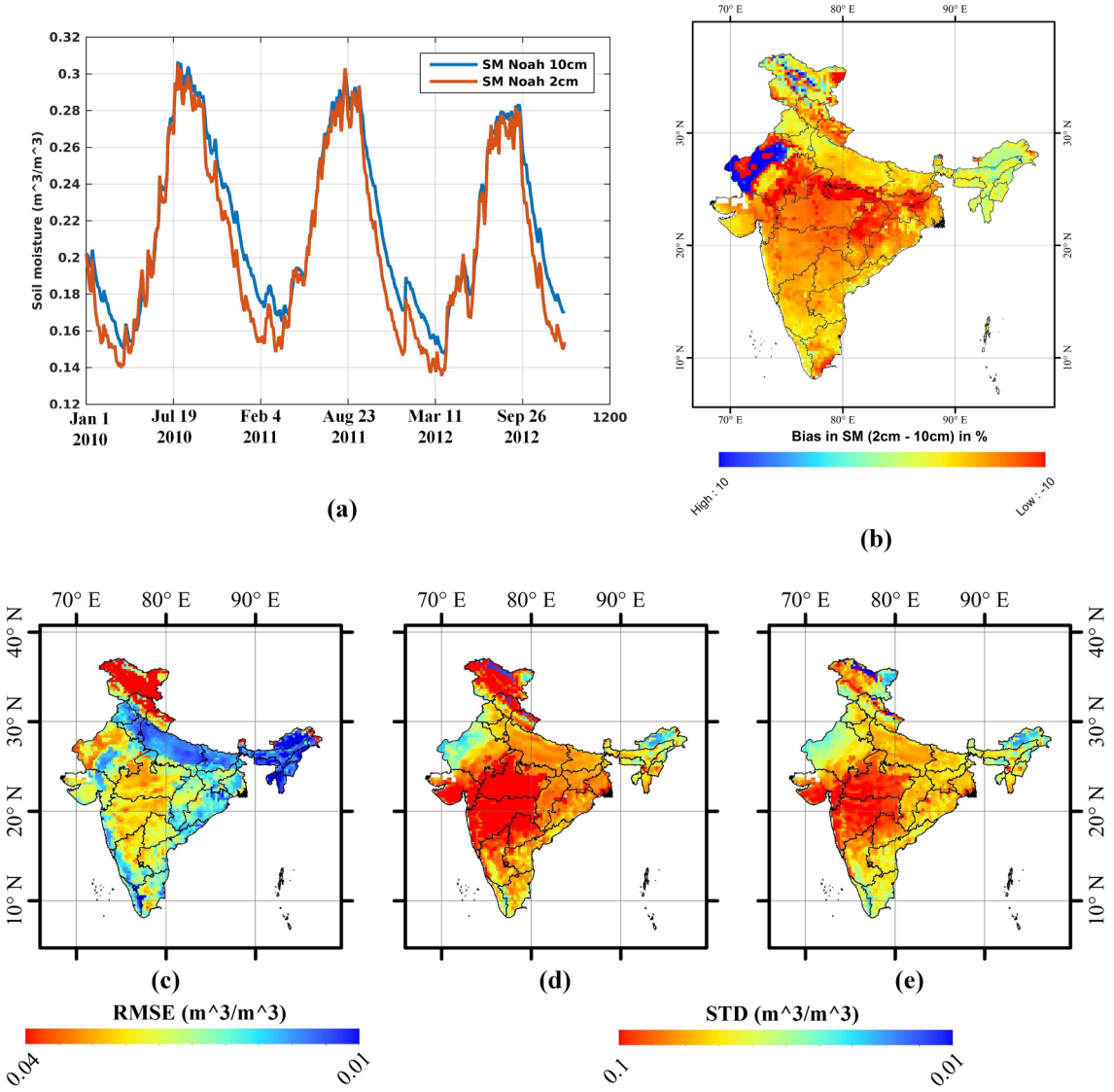

Fig. A1. Represents change in soil moisture with respect to change in first layer NOAH depth from 2 cm to 10 cm (a) Time series of SM from 2 cm and 10 cm, (b) Percentage bias in 2 cm simulated SM with respect to 10 cm SM, (c) RMSE in 2 cm SM with respect to 10 cm SM, (d) Standard deviation of 2 cm first layer SM, (e) same as d but for 10 cm first layer SM.

less than ± 5%, except few areas in Rajasthan having a bias of 9% and a few regions in central India at −7%. Furthermore, Fig. A.1(c) provides RMSE between SM simulation at 2 cm depth and 10 cm depth. It shows that maximum error is of around 0.04. Similarly, the 2 cm layer standard deviation (Fig. A.1d) and 10 cm layer standard deviation (Fig. A.1e) follows similar spatial patterns. Therefore, from this study, it can be concluded that changing the first layer depth to 2 cm has minimal impact on SM simulation of Noah LSM. This has motivated the authors to keep the first layer depth to a standard depth of 10 cm for all assimilation experiment.

References

Adegoke, J.O., Carleton, A.M., 2002. Relations between soil moisture and satellite vegetation indices in the U.S. Corn Belt. J. Hydrometeorol. 3, 395–405. https://doi.org/10.1175/1525-7541(2002) 003<0395:RBSMAS>2.0.CO;2.

Aghakouchak, A., Mehran, A., 2013. Extended contingency table: performance metrics for satellite observations and climate model simulations. Water Resour. Res. 49, 7144–7149. https://doi.org/10.1002/wrcr.20498.

Aghakouchak, A., Mehran, A., Norouzi, H., Behrangi, A., 2012. Systematic and random error components in satellite precipitation data sets. Geophys. Res. Lett. 39, 3–6. https://doi.org/10.1029/2012GL051592.

Ahmed, M., Sultan, M., Yan, E., Wahr, J., 2016. Assessing and improving land surface model outputs over Africa using GRACE, field, and remote sensing data. Surv. Geophys. 37, 529–556. https://doi.org/10.1007/s10712-016-9360-8.

Ambika, K.A., Mishra, V. 2016. figshare. https://dx.doi.org/10.6084/m9.figshare.3790611.v1.

Anderson, W.B., Zaitchik, B.F., Hain, C.R., Anderson, M.C., Yilmaz, M.T., Mecikalski, J., Schultz, L., 2012. Towards an integrated soil moisture drought monitor for East Africa. Hydrol. Earth Syst. Sci. 16, 2893–2913. https://doi.org/10.5194/hess-16-2893-2012.

Blankenship, C.B., Case, J.L., Crosson, W.L., Zavodsky, B.T., 2018. Correction of forcing-related spatial artifacts in a land surface model by satellite soil moisture data assimilation. IEEE Geosci. Remote Sens. Lett. 15, 498–502. https://doi.org/10.1109/LGRS.2018.2805259.

Bolten, J.D., Crow, W.T., Jackson, T.J., Zhan, X., Reynolds, C.A., 2010. Evaluating the utility of remotely sensed soil moisture retrievals for operational agricultural drought monitoring. IEEE J. Sel. Top. Appl. Earth Obs. Remote Sens. 3, 57–66. https://doi.org/10.1109/JSTARS.2009.2037163.

Botter, G., Peratoner, F., Porporato, A., Rodriguez-Iturbe, I., Rinaldo, A., 2007. Signatures of large-scale soil moisture dynamics on streamflow statistics across U.S. climate regimes. Water Resour. Res. 43, 1–10. https://doi.org/10.1029/2007WR006162.

Brocca, L., Tarpanelli, A., Filippucci, P., Dorigo, W., Zaussinger, F., Gruber, A., Fernández-Prieto, D., 2018. How much water is used for irrigation? A new approach exploiting coarse resolution satellite soil moisture products. Int. J. Appl. Earth Observ. Geoinf. 73, 752–766.

Caires, S., Sterl, A., 2003. Validation of ocean wind and wave data using triple collocation. J. Geophys. Res. Oceans 108, 3098. https://doi.org/10.1029/2002JC001491.

Chakravarti, M., Laha, I.G., Roy, J., 1967. Handbook of Methods of Applied Statistics. J. Royal Stat. Soc. Ser. A (General) 1. https://doi.org/10.2307/1267471.

Chen, F., Dudhia, J., 2001. Coupling an advanced land surface-hydrology model with the Penn State–NCAR MM5 modeling system. Part I: model implementation and sensitivity. Mon. Weather Rev. 129, 569–585. https://doi.org/10.1175/1520-0493(2001)129<0569:CAALSH>2.0.CO;2.

Chen, F., Mitchell, K., Schaake, J., Xue, Y., Pan, H.-L., Koren, V., Duan, Q.Y., Ek, M., Betts, A., 1996. Modeling of land surface evaporation by four schemes and comparison with FIFE observations. J. Geophys. Res. Atmos. 101, 7251–7268. https://doi.org/10.1029/95JD02165.

Ciabatta, L., Marra, A.C., Panegrossi, G., Casella, D., Sanò, P., Dietrich, S., Brocca, L., 2017. Daily precipitation estimation through different microwave sensors: verification study over Italy. J. Hydrol. 545, 436–450.

Corbari, C., Mancini, M., 2014. Calibration and validation of a distributed energy-water balance model using satellite data of land surface temperature and ground discharge measurements. J. Hydrometeorol. 15, 376–392. https://doi.org/10.1175/JHM-D-12-0173.1.

Corbari, C., Sobrino, J.A., Mancini, M., Hidalgo, V., 2010. Land surface temperature representativeness in a heterogeneous area through a distributed energy-water balance model and remote sensing data. Hydrol. Earth Syst. Sci. 14, 2141–2151. https://doi.org/10.5194/hess-14-2141-2010.

Crow, W.T., 2003. Multiobjective calibration of land surface model evapotranspiration predictions using streamflow observations and spaceborne surface radiometric temperature retrievals. J. Geophys. Res. 108, 4725. https://doi.org/10.1029/2002JD003292.

Crow, W.T., Van Den Berg, M.J., Huffman, G.J., Pellarin, T., 2011. Correcting rainfall using satellite-based surface soil moisture retrievals: the soil moisture analysis rainfall tool (SMART). Water Resour. Res. 47 (8).

De Lannoy, G.J.M., Reichle, R.H., 2016. Assimilation of SMOS brightness temperatures or soil moisture retrievals into a land surface model. Hydrol. Earth Syst. Sci. Discuss. 17, 1–27. https://doi.org/10.5194/hess-2016-414.

Derber, J.C., Parrish, D.F., Lord, S.J., 1991. The new global operational analysis system at the national meteorological center. Weather Forecast. 6, 538–547. https://doi.org/10.1175/1520-0434(1991) 006<0538:tngoas>2.0.co;2.

Dirmeyer, P.A., Halder, S., 2016. Sensitivity of numerical weather forecasts to initial soil moisture variations in CFSv2. Weather Forecast. 31, 1973–1983. https://doi.org/10.1175/WAF-D-16-0049.1.

Dorigo, W., Wagner, W., Albergel, C., Albrecht, F., Balsamo, G., Brocca, L., Chung, D., Ertl, M., Forkel, M., Gruber, A., Haas, E., Hamer, P.D., Hirschi, M., Ikonen, J., de Jeu, R., Kidd, R., Lahoz, W., Liu, Y.Y., Miralles, D., Mistelbauer, T., Nicolai-Shaw, N., Parinussa, R., Pratola, C., Reimer, C., van der Schalie, R., Seneviratne, S.I., Smolander, T., Lecomte, P., 2017. ESA CCI soil moisture for improved Earth system understanding: state-of-the art and future directions. Remote Sens. Environ. 203, 185–215. https://doi.org/10.1016/j.rse.2017.07.001.

Draper, C.S., Reichle, R.H., De Lannoy, G.J.M., Liu, Q., 2012. Assimilation of passive and active microwave soil moisture retrievals. Geophys. Res. Lett. 39, L04401. https://doi.org/10.1029/2011GL050655.

Draper, C., Reichle, R., de Jeu, R., Naeimi, V., Parinussa, R., Wagner, W., 2013. Estimating root mean square errors in remotely sensed soil moisture over continental scale domains. Remote Sens. Environ. 137, 288–298. https://doi.org/10.1016/j.rse.2013.06.013.

Entekhabi, D., Njoku, E.G., O'Neill, P.E., Kellogg, K.H., Crow, W.T., Edelstein, W.N., Entin, J.K., Goodman, S.D., Jackson, T.J., Johnson, J., Kimball, J., Piepmeier, J.R., Koster, R.D., Martin, N., McDonald, K.C., Moghaddam, M., Moran, S., Reichle, R., Shi, J.C., Spencer, M.W., Thurman, S.W., Tsang, L., Van Zyl, J., 2010. The soil moisture active passive (SMAP) mission. Proc. IEEE 98, 704–716. https://doi.org/10.1109/JPROC.2010.2043918.

Fernandez-Moran, R., Al-Yaari, A., Mialon, A., Mahmoodi, A., Al Bitar, A., De Lannoy, G., Rodriguez-Fernandez, N., Lopez-Baeza, E., Kerr, Y., Wigneron, J.-P., 2017a. SMOS-IC: an alternative SMOS Soil moisture and vegetation optical depth product. Remote Sens. 9, 457. https://doi.org/10.3390/rs9050457.

Fernandez-Moran, R., Wigneron, J.-P., De Lannoy, G., Lopez-Baeza, E., Parrens, M., Mialon, A., Mahmoodi, A., Al-Yaari, A., Bircher, S., Al Bitar, A., Richaume, P., Kerr, Y., 2017b. A new calibration of the effective scattering albedo and soil roughness parameters in the SMOS SM retrieval algorithm. Int. J. Appl. Earth Obs. Geoinf. 62, 27–38. https://doi.org/10.1016/j.jag.2017.05.013.

Figa-Saldaña, J., Wilson, J.J.W., Attema, E., Gelsthorpe, R., Drinkwater, M.R., Stoffelen, A., 2002. The advanced scatterometer (ASCAT) on the meteorological operational (MetOp) platform: a follow on for European wind scatterometers. Can. J. Remote Sens. 28, 404–412. https://doi.org/10.5589/m02-035.

Franks, S.W., Beven, K.J., 1999. Conditioning a multiple-patch SVAT model using uncertain time-space estimates of latent heat fluxes as inferred from remotely sensed data. Water Resour. Res. 35, 2751–2761. https://doi.org/10.1029/1999WR900108.

Franks, S.W., Beven, K.J., Quinn, P.F., Wright, I.R., 1997. On the sensitivity of soil-vegetation-atmosphere transfer (SVAT) schemes: equifinality and the problem of robust calibration. Agric. For. Meteorol. 86, 63–75. https://doi.org/10.1016/S0168-1923(96)02421-5.

Gaiser, P.W., St. Germain, K.M., Twarog, E.M., Poe, G.A., Purdy, W., Richardson, D., Grossman, W., Jones, W.L., Spencer, D., Golba, G., Cleveland, J., Choy, L., Bevilacqua, R.M., Chang, P.S., 2004. The WindSat spaceborne polarimetric microwave radiometer: sensor description and early orbit performance. IEEE Trans. Geosci. Remote Sens. 42, 2347–2361. https://doi.org/10.1109/TGRS.2004.836867.

Gentemann, C.L., 2014. Three way validation of MODIS and AMSR-E sea surface temperatures. J. Geophys. Res. Oceans 119, 2583–2598. https://doi.org/10.1002/2013JC009716.

Gruber, A., Dorigo, W.A., Crow, W., Wagner, W., 2017. Triple collocation-based merging of satellite soil moisture retrievals. IEEE Trans. Geosci. Remote Sens. 55, 6780–6792. https://doi.org/10.1109/TGRS.2017.2734070.

Gupta, H.V., Bastidas, L.A., Sorooshian, S., Shuttleworth, W.J., Yang, Z.L., 1999. Parameter estimation of a land surface scheme using multicriteria methods. J. Geophys. Res. Atmos. 104, 19491–19503. https://doi.org/10.1029/1999JD900154.

Gutmann, E.D., Small, E.E., 2010. A method for the determination of the hydraulic properties of soil from MODIS surface temperature for use in land-surface models. Water Resour. Res. 46, 1–16. https://doi.org/10.1029/2009WR008203.

Han, E., Crow, W.T., Holmes, T., Bolten, J., 2014. Benchmarking a soil moisture data assimilation system for agricultural drought monitoring. J. Hydrometeorol. 15, 1117–1134. https://doi.org/10.1175/JHM-D-13-0125.1.

Imaoka, K., Kachi, M., Kasahara, M., Ito, N., Nakagawa, K., Oki, T., 2010. Instrument performance and calibration of AMSR-E and AMSR2. Int. Arch. Photogramm. Remote Sens. Spat. Inf. Sci. - ISPRS Arch. 38, 13–16.

Jain, M., Mondal, P., Galford, G.L., Fiske, G., DeFries, R.S., 2017. India Annual Winter Cropped Area, 2001-2016. NASA Socioeconomic Data and Applications Center (SEDAC), Palisades NY 10.7927/H47D2S3W. Accessed 02 November 2018.

Karthikeyan, L., Pan, M., Wanders, N., Kumar, D.N., Wood, E.F., 2017a. Four decades of microwave satellite soil moisture observations: Part 2. Product validation and inter-satellite comparisons. Adv. Water Resour. 109, 236–252. https://doi.org/10.1016/j.advwatres.2017.09.010.

Karthikeyan, L., Pan, M., Wanders, N., Kumar, D.N., Wood, E.F., 2017b. Four decades of microwave satellite soil moisture observations: Part 1. A review of retrieval algorithms. Adv. Water Resour. 109, 106–120. https://doi.org/10.1016/j.advwatres.2017.09.006.

Kerr, Y.H., Waldteufel, P., Wigneron, J.-P., Delwart, S., Cabot, F., Boutin, J., Escorihuela,

M.-J., Font, J., Reul, N., Gruhier, C., Juglea, S.E., Drinkwater, M.R., Hahne, A., Martín-Neira, M., Mecklenburg, S., 2010. The SMOS mission: new tool for monitoring key elements of the global water cycle. Proc. IEEE 98, 666–687. https://doi.org/10.1109/JPROC.2010.2043032.

Kolassa, J., Gentine, P., Prigent, C., Aires, F., Alemohammad, S.H., 2017. Soil Moisture retrieval from AMSR-R and ASCAT microwave observations synergy. Part2: product evaluation. Remote Sens. Environ. 195 (2017), 202–217.

Koster, R.D., Dirmeyer, P.A., Guo, Z., Bonan, G., Chan, E., Cox, P., Gordon, C.T., Kanae, S., Kowalczyk, E., Lawrence, D., Liu, P., Lu, C.-H., Malyshev, S., McAvaney, B., Mitchell, K., Mocko, D., Oki, T., Oleson, K., Pitman, A., Sud, Y.C., Taylor, C.M., Verseghy, D., Vasic, R., Xue, Y., Yamada, T., 2004. Regions of strong coupling between soil moisture and precipitation. Science (80) 305, 1138–1140. https://doi.org/10.1126/science.1100217.

Krishnamurthy, V., Shukla, J., 2000. Intraseasonal and interannual variability of rainfall over India. J. Clim. 13, 4366–4377.

Kumar, S.V., Peters-Lidard, C.D., Santanello, J.A., Reichle, R.H., Draper, C.S., Koster, R.D., Nearing, G., Jasinski, M.F., 2015. Evaluating the utility of satellite soil moisture retrievals over irrigated areas and the ability of land data assimilation methods to correct for unmodeled processes. Hydrol. Earth Syst. Sci. Discuss. 12, 5967–6009. https://doi.org/10.5194/hessd-12-5967-2015.

Kumar, S., Reichle, R., Harrison, K., Peters-Lidard, C., Yatheendradas, S., Santanello, J., 2012. A comparison of methods for a priori bias correction in soil moisture data assimilation. Water Resour. Res. 48. https://doi.org/10.1029/2010WR010261.

Kumar, S., Reichle, R., Koster, R., Crow, W., Peters-Lidard, C., 2009. Role of subsurface physics in the assimilation of surface soil moisture observations. J. Hydrometeorol. 10, 1534–1547. https://doi.org/10.1175/2009JHM1134.1.

Kumar, S.V., Peters-Lidard, C.D., Tian, Y., Houser, P.R., Geiger, J., Olden, S., Lighty, L., Eastman, J.L., Doty, B., Dirmeyer, P., Adams, J., Mitchell, K., Wood, E.F., Sheffield, J., 2006. Land information system: an interoperable framework for high resolution land surface modeling. Environ. Model. Software 21, 1402–1415. https://doi.org/10.1016/j.envsoft.2005.07.004.

Kumar, S.V., Harrison, K.W., Peters-Lidard, C.D., Santanello Jr., J.A., Kirschbaum, D., 2014. Assessing the impact of L-band observations on drought and flood risk estimation: a decision-theoretic approach in an OSSE environment. J. Hydrometeorol. 15, 2140–2156. https://doi.org/10.1175/JHM-D-13-0204.1.

Lawston, P.M., Santanello, J.A., Kumar, S.V., 2017. Irrigation signals detected from SMAP soil moisture retrievals. Geophys. Res. Lett. 44 (23), 11860–11867.

Liang, X., Lettenmaier, D.P., Wood, E.F., Burges, S.J., 1994. A simple hydrologically based model of land surface water and energy fluxes for general circulation models. J. Geophys. Res. Atmos. 99, 14415–14428. https://doi.org/10.1029/94JD00483.

Lievens, H., Al Bitar, A., Verhoest, N.E.C., Cabot, F., De Lannoy, G.J.M., Drusch, M., Dumedah, G., Hendricks Franssen, H.-J., Kerr, Y., Tomer, S.K., Martens, B., Merlin, O., Pan, M., van den Berg, M.J., Vereecken, H., Walker, J.P., Wood, E.F., Pauwels, V.R.N., 2015a. Optimization of a radiative transfer forward operator for simulating SMOS brightness temperatures over the Upper Mississippi Basin. J. Hydrometeorol. 16, 1109–1134. https://doi.org/10.1175/JHM-D-14-0052.1.

Lievens, H., De Lannoy, G.J.M., Al Bitar, A., Drusch, M., Dumedah, G., Hendricks Franssen, H.J., Kerr, Y.H., Tomer, S.K., Martens, B., Merlin, O., Pan, M., Roundy, J.K., Vereecken, H., Walker, J.P., Wood, E.F., Verhoest, N.E.C., Pauwels, V.R.N., 2015b. Assimilation of SMOS soil moisture and brightness temperature products into a land surface model. Remote Sens. Environ. 180, 292–304. https://doi.org/10.1016/j.rse.2015.10.033.

Liu, D., Mishra, A.K., 2017. Performance of AMSR_E soil moisture data assimilation in CLM4.5 model for monitoring hydrologic fluxes at global scale. J. Hydrol. 547, 67–79. https://doi.org/10.1016/j.jhydrol.2017.01.036.

Liu, D., Wang, G., Mei, R., Yu, Z., Gu, H., 2014. Diagnosing the strength of land-atmosphere coupling at subseasonal to seasonal time scales in Asia. J. Hydrometeorol. 15, 320–339. https://doi.org/10.1175/JHM-D-13-0104.1.

Liu, Y.Y., Dorigo, W.A., Parinussa, R.M., De Jeu, R.A.M., Wagner, W., McCabe, M.F., Evans, J.P., Van Dijk, A.I.J.M., 2012. Trend-preserving blending of passive and active microwave soil moisture retrievals. Remote Sens. Environ. 123, 280–297. https://doi.org/10.1016/j.rse.2012.03.014.

Luo, L., Wood, E.F., 2007. Monitoring and predicting the 2007 U.S. drought. Geophys. Res. Lett. 34, 1–6. https://doi.org/10.1029/2007GL031673.

Mahrt, L., Ek, M., 1984. The influence of atmospheric stability on potential evaporation. J. Clim. Appl. Meteorol. https://doi.org/10.1175/1520-0450(1984)023<0222:TIOASO>2.0.CO;2.

McColl, K.A., Alemohammad, S.H., Akbar, R., Konings, A.G., Yueh, S., Entekhabi, D., 2017. The global distribution and dynamics of surface soil moisture. Nat. Geosci. 10, 100–104. https://doi.org/10.1038/ngeo2868.

Miralles, D.G., Teuling, A.J., Van Heerwaarden, C.C., De Arellano, J.V.G., 2014. Mega-heatwave temperatures due to combined soil desiccation and atmospheric heat accumulation. Nat. Geosci. 7, 345–349. https://doi.org/10.1038/ngeo2141.

Mishra, V., Shah, R., Azhar, S., Shah, H., Modi, P., Kumar, R., 2017. Reconstruction of droughts in India using multiple land surface models (1951-2015). Hydrol. Earth Syst. Sci. 1–22.

Mitchell, K.E., 2004. The multi-institution North American Land Data Assimilation System (NLDAS): Utilizing multiple GCIP products and partners in a continental distributed hydrological modeling system. J. Geophys. Res. 109, D07S90. https://doi.org/10.1029/2003JD003823.

Nair, A.S., Indu, J., 2018a. Utilizing GRACE and GLDAS data for estimating groundwater storage variability over the Krishna Basin. ISPRS Ann. Photogramm. Remote Sens. Spatial Inf. Sci. 45, 129–136.

Nair, A.S., Indu, J., 2018b. A coupled land surface and radiative transfer models based on relief correction for a reliable land data assimilation over mountainous terrain. IEEE Geosci. Remote Sens. Lett. 15 (11), 1657–1661.

Nair, A.S., Indu, J., 2017. Performance assessment of multi-source weighted-ensemble precipitation (MSWEP) product over India. Climate 5, 1–20. https://doi.org/10.3390/cli5010002.

Nair, A.S., Indu, J., 2016. Enhancing Noah land surface model prediction skill over indian subcontinent by assimilating SMOPS blended soil moisture. Remote Sens. https://doi.org/10.3390/rs8120976.

Njoku, E.G., Jackson, T.J., Lakshmi, V., Chan, T.K., Nghiem, S.V., 2003. Soil moisture retrieval from AMSR-E. IEEE Trans. Geosci. Remote Sens. 41, 215–228. https://doi.org/10.1109/TGRS.2002.808243.

O'Carroll, A.G., Eyre, J.R., Saunders, R.W., 2008. Three-way error analysis between AATSR, AMSR-E, and in situ sea surface temperature observations. J. Atmos. Ocean. Technol. 25, 1197–1207. https://doi.org/10.1175/2007JTECHO542.1.

Orth, R., Seneviratne, S.I., 2013. Propagation of soil moisture memory to streamflow and evapotranspiration in Europe. Hydrol. Earth Syst. Sci. 17, 3895–3911. https://doi.org/10.5194/hess-17-3895-2013.

Pai, D.S., Sridhar, L., Rajeevan, M., Sreejith, O.P., Satbhai, N.S., Mukhopadyay, B., 2014. Development of a new high spatial resolution (0. 25° × 0. 25°) Long Period (1901–2010) daily gridded rainfall data set over India and its comparison with existing data sets over the region. Mausam 65, 1–18.

Parinussa, R.M., Lakshmi, V., Johnson, F.M., Sharma, A., 2016. A new framework for monitoring flood inundation using readily available satellite data. Geophys. Res. Lett 2599–2605. https://doi.org/10.1002/2016GL068192.Received.

Pellarin, T., Louvet, S., Gruhier, C., Quantin, G., Legout, C., 2013. A simple and effective method for correcting soil moisture and precipitation estimates using AMSR-E measurements. Remote Sens. Environ. 136, 28–36.

Peters-Lidard, C.D., Houser, P.R., Tian, Y., Kumar, S.V., Geiger, J., Olden, S., Lighty, L., Doty, B., Dirmeyer, P., Adams, J., Mitchell, K., Wood, E.F., Sheffield, J., 2007. High-performance Earth system modeling with NASA/GSFC's Land Information System. Innov. Syst. Software Eng. 3, 157–165. https://doi.org/10.1007/s11334-007-0028-x.

Reichle, R., Koster, R., Liu, P., Mahanama, S., Njoku, E., Owe, M., 2007. Comparison and assimilation of global soil moisture retrievals from the advanced microwave scanning radiometer for the earth observing system (AMSR-E) and the scanning multichannel microwave radiometer (SMMR). J. Geophys. Res. Atmos. 112, D09108. https://doi.org/10.1029/2006JD008033.

Reichle, R., McLaughlin, D.B., Entekhabi, D., 2002. Hydrologic data assimilation with the ensemble Kalman filter. Mon. Weather Rev. 130, 103–114. https://doi.org/10.1175/1520-0493(2002)130<0103:HDAWTE>2.0.CO;2.

Reichle, R.H., Koster, R.D., 2005. Global assimilation of satellite surface soil moisture retrievals into the NASA catchment land surface model. Geophys. Res. Lett. 32, 1–4. https://doi.org/10.1029/2004GL021700.

Reichle, R.H., Koster, R.D., 2004. Bias reduction in short records of satellite soil moisture. Geophys. Res. Lett. 31, 2–5. https://doi.org/10.1029/2004GL020938.

Rodell, M., Houser, P.R., Jambor, U., Gottschalck, J., Mitchell, K., Meng, C.-J., Arsenault, K., Cosgrove, B., Radakovich, J., Bosilovich, M., Entin, J.K., Walker, J.P., Lohmann, D., Toll, D., 2004. The global land data assimilation system. Bull. Am. Meteorol. Soc. 85, 381–394. https://doi.org/10.1175/BAMS-85-3-381.

Roebeling, R.A., Wolters, E.L.A., Meirink, J.F., Leijnse, H., 2012. Triple collocation of summer precipitation retrievals from SEVIRI over Europe with gridded rain gauge and weather radar data. J. Hydrometeorol. 13, 1552–1566. https://doi.org/10.1175/JHM-D-11-089.1.

Salvucci, G.D., 2001. Using conditionally averaged precipitation. Water Resour. 37, 1357–1365.

Scipal, K., Holmes, T., de Jeu, R., Naeimi, V., Wagner, W., 2008. A possible solution for the problem of estimating the error structure of global soil moisture data sets. Geophys. Res. Lett. 35. https://doi.org/10.1029/2008GL035599.

Sellers, P.J., Dickinson, R.E., Randall, D.A., Betts, A.K., Hall, F.G., Berry, J.A., Collatz, G.J., Denning, A.S., Mooney, H.A., Nobre, C.A., Sato, N., Field, C.B., Henderson-Sellers, A., 1997. Modeling the exchange of energy, water, and carbon between continents and atmosphere. Science (80-.) 275, 602–609.

Shellito, P.J., Small, E.E., Cosh, M.H., 2016. Calibration of Noah soil hydraulic property parameters using surface soil moisture from SMOS and Basinwide in situ observations. J. Hydrometeorol. 17, 2275–2292. https://doi.org/10.1175/JHM-D-15-0153.1.

Shellito, P.J., Small, E.E., Livneh, B., 2018. Controls on surface soil drying rates observed by SMAP and simulated by the Noah land surface model. Hydrol. Earth Syst. Sci. 22, 1649–1663. https://doi.org/10.5194/hess-22-1649-2018.

Sorooshian, S., Lawford, R., Try, P., 2005. Water and energy cycles: Investigating the links. World Meteorol. 1–7.

Stoffelen, A., 1998. Toward the true near-surface wind speed: error modeling and calibration using triple collocation. J. Geophys. Res. 103, 7755–7766.

Tian, X., Xie, Z., Dai, A., Jia, B., Shi, C., 2010. A microwave land data assimilation system: scheme and preliminary evaluation over China. J. Geophys. Res. Atmos. 115, 1–13. https://doi.org/10.1029/2010JD014370.

Wagner, W., Hahn, S., Kidd, R., Melzer, T., Bartalis, Z., Hasenauer, S., Figa-Saldaña, J., De Rosnay, P., Jann, A., Schneider, S., Komma, J., Kubu, G., Brugger, K., Aubrecht, C., Züger, J., Gangkofner, U., Kienberger, S., Brocca, L., Wang, Y., Blöschl, G., Eitzinger, J., Steinnocher, K., Zeil, P., Rubel, F., 2013. The ASCAT soil moisture product: a review of its specifications, validation results, and emerging applications. Meteorol. Z. 22, 5–33. https://doi.org/10.1127/0941-2948/2013/0399.

Wang, X., Xie, H., Guan, H., Zhou, X., 2007. Different responses of MODIS-derived NDVI

to root-zone soil moisture in semi-arid and humid regions. J. Hydrol. 340, 12–24. https://doi.org/10.1016/j.jhydrol.2007.03.022.
Wigneron, J.-P., Kerr, Waldteufel, P., Saleh, K., Escorihuela, M.-J., Richaume, P., Ferrazzoli, P., de Rosnay, P., Gurney, R., Calvet, J.-C., Grant, J.P., Guglielmetti, M., Hornbuckle, B., Mätzler, C., Pellarin, T., Schwank, M., 2007. L-band microwave emission of the biosphere (L-MEB) model: description and calibration against experimental data sets over crop fields. Remote Sens. Environ. 107, 639–655.
Zaitchik, B.F., Rodell, M., Olivera, F., 2010. Evaluation of the global land data assimilation system using global river discharge data and a source-to-sink routing scheme. Water Resour. Res. 46, 1–17. https://doi.org/10.1029/2009WR007811.
Zhao, L., Yang, Z.L., Hoar, T.J., 2016. Global soil moisture estimation by assimilating AMSR-E brightness temperatures in a coupled CLM4–RTM–DART system. J. Hydrometeorol. 17, 2431–2454. https://doi.org/10.1175/JHM-D-15-0218.1.